“Sea Surface Temperature Variability: Patterns and Mechanisms”

Clara Deser, Michael A. Alexander, Shang-Ping Xie and Adam S. Phillips

Submitted to *Annual Review of Marine Sciences, Vol. 2*

April 30, 2009

Key Words

Ocean-atmosphere interaction, El Niño, Pacific Decadal Oscillation, Atlantic Multidecadal Oscillation, climate variability

Abstract

Patterns of sea surface temperature (SST) variability on inter-annual and longer time scales result from a combination of atmospheric and oceanic processes. These SST anomaly patterns may be due to intrinsic modes of atmospheric circulation variability which imprint themselves upon the SST field mainly via surface energy fluxes. Examples include: SST fluctuations in the Southern Ocean associated with the Southern Annular Mode; a tri-polar pattern of SST anomalies in the North Atlantic associated with the North Atlantic Oscillation; and a pan-Pacific mode known as the Pacific Decadal Oscillation (with additional contributions from oceanic processes). They may also result from coupled ocean-atmosphere interactions, such as the El Niño/Southern Oscillation phenomenon in the tropical Indo-Pacific, the tropical Atlantic Niño, and the cross-equatorial meridional modes in the tropical Pacific and Atlantic. Finally, patterns of SST variability may arise from intrinsic oceanic modes, notably the Atlantic Multidecadal Oscillation.

1. Introduction

The oceans play an important role in the climate system due in part to their large heat storage capacity: approximately 2.5 m of water contains as much energy as an entire atmospheric column. The oceans' thermal inertia is communicated to the atmosphere via

turbulent and radiative energy exchange at the sea surface. These energy fluxes in turn depend on a single oceanic quantity, the sea surface temperature (SST), as well as several atmospheric parameters including wind speed, air temperature, humidity, and cloudiness. SSTs thus play a key role in regulating climate and its variability. In particular, slow variations in SST provide a source of potential predictability for climate fluctuations on time scales of seasons and longer. In this review, we describe the dominant spatial and temporal patterns of non-seasonal SST variability observed over the past ~150 years, and discuss the current state of knowledge regarding their underlying physical mechanisms and climate impacts.

The rest of the paper is outlined as follows. Section 2 provides some background on the physical processes governing SST variability, including the role of atmospheric circulation forcing. The North Atlantic SST tripole mode is used to illustrate the latter. Section 3 introduces the SST data sets commonly used for climate studies, with an emphasis on issues related to spatial and temporal coverage. Section 4 discusses the geographical distribution of non-seasonal SST variability and provides a brief introduction to Empirical Orthogonal Function analysis, a commonly used technique for identifying patterns of variability. Section 5 presents the primary modes of non-seasonal SST variability in each ocean basin. These include (in addition to the North Atlantic SST tripole): 1) the El Niño/Southern Oscillation (ENSO) phenomenon in the tropical Pacific, with teleconnections to the other ocean basins; 2) the tropical Indian Ocean dipole mode; 3) the tropical Atlantic Niño and meridional modes; 4) Southern Ocean variability; 5) the Pacific Decadal Oscillation; and 6) the Atlantic Multi-decadal Oscillation. A summary and outlook are provided in Sections 6 and 7, respectively.

2. Physical Background

a. Heat Budget of the Upper Ocean Mixed Layer

SSTs are governed by both atmospheric and oceanic processes. On the atmospheric side, wind speed, air temperature, cloudiness, and humidity are the dominant factors regulating the exchange of energy at the sea surface. On the oceanic side, heat transport by currents, vertical mixing, and boundary layer depth influence SST. Mathematically, the heat budget for the upper-ocean mixed layer may be written as:

$$dT/dt = Qnet/(\rho CpH) + (Ugeo+Uek)\cdot \nabla T + (We+Wek)(T-Tb)/H \qquad \text{Eq 1}$$

where ρ is the density of seawater, Cp is the specific heat of seawater, H is the mixed layer depth, T is the mixed layer temperature (equal to the SST), Qnet is the net surface energy flux, Ugeo is the geostrophic current velocity, Uek is the Ekman current velocity, We is the vertical entrainment rate, Wek is the Ekman pumping velocity, and Tb is the temperature of the water at depth that is entrained into the mixed layer. Qnet is defined as:

$$Qnet = Qsh + Qlh + Qsw + Qlw \qquad \text{Eq 2}$$

where Qsh is the sensible heat flux, Qlh is the latent heat flux, Qsw is the downward solar radiative flux minus the portion that penetrates through the mixed layer, and Qlw is the longwave radiative flux. The turbulent (Qsh + Qlh) energy flux is linearly proportional to the wind speed, the air-sea temperature (Qsh) and the air-sea humidity difference (Qlh); the radiative fluxes (Qsw + Qlh) are functions of air temperature, humidity, and cloudiness. The bulk formulae for the air-sea fluxes may be found in standard texts such as Peixoto and Oort (1992), Pond and Pickard (1983) and Hartmann (1994). Ekman and

geostrophic currents contribute to the heat budget of the mixed layer through horizontal advection, while entrainment and Ekman pumping alter the SST through vertical advection. A complete discussion of these terms may be found in standard oceanography texts such as Pond and Pickard (1983), Vallis (2006), and Stewart (2005).

b. Atmospheric Circulation Forcing

Much of the large-scale organization of SST anomalies results from the large-scale organization of atmospheric circulation anomalies and attendant changes in the turbulent and radiative energy fluxes at the air-sea interface and the local wind-driven Ekman currents (Cayan, 1992; Alexander and Scott, 1997; Deser and Timlin, 1997; Marshall et al., 2001; Visbeck et al., 2003; Alexander and Scott, 2008). In the middle latitudes, eastward moving storms dominate surface energy flux variations on synoptic time scales (3 to 10 days), while blocking events, slowly moving cutoff lows, Rossby waves, and semi-stationary patterns contribute to surface energy flux variations on time scales longer than about 10 days (Alexander and Scott, 1997). In general, atmospheric variability with time scales longer than about 10 days is more effective at driving SST anomalies than synoptic atmospheric variability due to the thermal inertia of the upper ocean mixed layer (Frankignoul and Hasselmann, 1977; Deser et al., 2003). The frequency-dependence of the thermal response of the mixed layer to atmospheric forcing will be discussed further below.

Extra-tropical atmospheric circulation variability on time scales longer than about 10 days tends to be organized into recurring large-scale patterns anchored to particular geographical regions. These large-scale patterns often consist of anomalies of opposite

sign over distant parts of the globe, commonly referred to as "teleconnections" in the meteorological literature (Wallace and Gutzler, 1981; Barnston and Livezey, 1987; Kushnir and Wallace, 1989, Trenberth et al., 1998). Prominent examples of large-scale teleconnection patterns of extra-tropical atmospheric circulation variability include: the North Atlantic Oscillation (NAO) and the related Northern Annular Mode (NAM); the Pacific-North American (PNA) and Pacific-South American (PSA) patterns; and the Southern Annular Mode (SAM). Nigam (2003) reviews these and other atmospheric circulation teleconnection patterns.

The NAO refers to a redistribution of atmospheric mass, manifest as sea level pressure (SLP) changes of opposite sign, between the Arctic and subtropics of the Atlantic sector (e.g., Figure 1). This SLP oscillation (in space, not time: Walker and Bliss, 1932) is accompanied by changes in wind, storminess, air temperature and precipitation across the North Atlantic as well as over eastern North America and Europe (see Hurrell and Deser, 2009 for a recent review). The related NAM incorporates the spatial pattern of the NAO with a third center of SLP variability over the North Pacific that fluctuates in phase with that over the North Atlantic. The NAM's southern hemisphere counterpart, the SAM, also refers to a north-south redistribution of atmospheric mass between high (poleward of 50°S) and middle (30° - 50°S) latitudes, with accompanying changes in wind, air temperature, and precipitation (Marshall, 2003). The SAM is a zonally symmetric pattern of atmospheric circulation variability that spans all longitudes whereas the NAM exhibits more zonal variation due to continental effects (Thompson and Wallace, 2000). Finally, the PNA and PSA are wave-like teleconnection patterns consisting of SLP anomaly centers that approximately follow a 'great circle

route' over the Pacific and American sectors of their respective hemispheres (Wallace and Gutzler, 1981; Karoly, 1989). Most prominent during winter, these patterns affect wind, air temperature, and precipitation over the North and South Pacific.

The spatial structures of these large-scale patterns of extra-tropical atmospheric circulation variability are driven primarily by internal non-linear dynamical processes. That is, they are intrinsic to the atmosphere and require no external forcing to exist. The temporal evolution of these atmospheric circulation patterns is generally consistent with a stochastic first-order autoregressive process with an e-folding time scale of about 10 days (Feldstein, 2000; Johnson and Feldstein, 2009). That is, these patterns tend to follow a random sequence akin to white noise on time scales longer than about 10 days. Although these teleconnection patterns are intrinsic to the atmosphere, they may also be excited by external forcing factors such as changes in SSTs, sea ice, atmospheric chemical composition (for example, volcanic aerosols, and ozone and greenhouse gas concentrations) and solar output, in analogy with the excitation of the "normal modes" of a drum. These external forcings may thus alter the temporal evolution of atmospheric teleconnection patterns, enhancing their persistence and potential predictability. External forcing may also generate new patterns of atmospheric circulation response.

In contrast to the extra-tropics, large-scale patterns of atmospheric circulation variability in the tropics result primarily from interaction with the ocean: that is, they do not exist in the absence of SST variability. The most prominent large-scale tropical atmospheric pattern of variability is the Southern Oscillation (SO), an east-west redistribution of atmospheric mass between the Indian Ocean/western Pacific and the eastern Pacific. In the positive (negative) phase of the SO, the SLP gradient across the

tropical Pacific is stronger (weaker) than normal, accompanied by enhanced (diminished) Trade Winds and equatorial easterly winds. This pattern owes its existence to tropical ocean-atmosphere interaction associated with the El Niño – Southern Oscillation (ENSO) phenomenon and is thus an intrinsically coupled phenomenon. The roles of intrinsic and ocean-coupled atmospheric variability are discussed further in connection with specific patterns of SST variability.

The large-scale nature of atmospheric teleconnection patterns is imprinted upon the sea surface temperature anomaly field via the surface energy fluxes and Ekman currents. This is illustrated for the NAO in Figure 1. The top left panel shows the winter (December-March) SST, SLP and surface wind anomaly regression maps associated with a +1 standard deviation departure of the NAO defined using the station index of Hurrell et al. (2003). The SST field exhibits a tri-polar structure marked by a cold anomaly in the sub-polar North Atlantic, a warm anomaly in the middle latitudes, and a cold subtropical anomaly between the equator and 30°N; warm anomalies are also found in the Greenland and North Seas. Maximum SST anomaly amplitudes are on the order of 0.5°C. A similar tri-polar pattern is seen in the turbulent energy fluxes (Figure 1; top right panel), where the sign is defined as positive downwards (e.g., from the atmosphere to the ocean). The ocean loses energy to the atmosphere over the sub-polar and tropical Atlantic due to strengthened westerly winds and northeast Trade winds, respectively; and it gains energy in the middle latitudes due to the diminished wind speeds (easterly anomalies superimposed upon a background of mean westerlies) and anomalous warm air advection associated with southerly wind anomalies along the eastern seaboard of the United States. Thus, the large-scale structure of the SST anomaly tripole is driven by the turbulent

energy flux anomalies associated with the NAO (e.g., Cayan; 1992; Marshall et al., 2001; and Visbeck et al., 2003). While the mixed layer heat budget equation relates the fluxes to the time-tendency of SST and not the SST per se (recall Eqn. 1), it has been shown that the winter-mean SST anomaly closely resembles the SST anomaly tendency across the winter season, and that the SST anomalies lag the atmospheric forcing by 2-3 weeks (e.g., Deser and Timlin, 1997).

Although the surface turbulent energy fluxes drive the overall tri-polar pattern of SST anomalies associated with the NAO, horizontal temperature advection by the anomalous Ekman currents, expressed as an equivalent surface heat flux anomaly, also contributes in regions of strong mean SST gradients such as the Gulf Stream and North Atlantic Current (Figure 1, lower left). Other factors such as the radiative fluxes at lower latitudes and spatial variations in mixed layer depth also play a role in determining the magnitude of the SST anomalies (not shown). For example, the winter mixed layers are substantially deeper in the sub-polar North Atlantic compared to the tropical Atlantic (~ 300m compared to ~60m) which reduces the amplitude of the SST response (recall Eqn. 1). This effect is evidenced by the fact that the NAO-related SST anomalies are of comparable magnitude between high and low latitudes whereas the heat flux anomalies differ by approximately a factor of 5 (Figure 1). Although the SST anomalies associated with the North Atlantic tripole are primarily forced by the atmosphere, there is some evidence for a weak feedback upon the NAO (Watanabe and Kimoto, 2000; Czaja and Frankignoul, 2002).

An important concept for understanding the nature of SST variability is the stochastic climate model paradigm (Frankignoul and Hasselmann, 1977). According to

this paradigm, ocean mixed layer temperature anomalies are forced by random atmospheric variability (e.g., atmospheric circulation variability that decorrelates within a week or two) *via* surface heat fluxes and Ekman currents, and decay by damping back to the atmosphere (modeled as a negative linear feedback term). Put another way, the ocean mixed layer integrates the "white noise" atmospheric forcing to yield a "red noise" SST response. In this view, the predictability or persistence of SST anomalies is limited to the timescale associated with the thermal inertia of the mixed layer, a timescale determined by the depth of the mixed layer and the rate at which the SST anomaly damps to the atmosphere via turbulent heat fluxes. The simple stochastic climate model has been widely adopted as the leading paradigm for the "null hypothesis" of SST variability in middle and high latitudes where random atmospheric forcing is a good approximation.

An illustration of the simple stochastic climate model paradigm is given in Figure 2 which shows the mixed layer temperature response to random variations in surface heat flux forcing over a 60 year period. Two cases are considered: a shallow (50m) and a deep (500m) mixed layer. These values span the typical range of observed mixed layer depths, with 50m being representative of annual mean conditions in the North Pacific and 500m typical of the northern North Atlantic during winter. Slow variations in the mixed layer temperature are apparent for both cases, with fluctuations on the order of a few years for the shallow case and on the order of decades for the deep mixed layer case. This simple example illustrates that slow SST variations may be induced by random (e.g., unpredictable) atmospheric forcing simply due to the thermal inertia associated with a deep mixed layer. Note that the stochastic climate model does not generate spectral peaks; rather it enhances the low-frequency component of variability according to a first-

order autoregressive process. The stochastic climate model paradigm has been shown to contribute to SST variability in the North Pacific associated with the "Pacific Decadal Oscillation" (Newman et al., 2003) and to the long (decadal time-scale) persistence of SST fluctuations in the North Atlantic (Deser et al., 2003; DeCoetlogon and Frankignoul, 2003). This powerful "null hypothesis" of SST variability makes it difficult to separate the contributions of oceanic and atmospheric forcing solely on the basis of time scale.

In addition to atmospheric processes, oceanic processes such as upwelling, entrainment and lateral advection also contribute to SST variability. For example, vertical advection plays a prominent role along the coastal and equatorial upwelling zones, and horizontal advection is important along the western boundary current regions (e.g., the Gulf Stream and Kuroshio Current). Oceanic processes also play an indirect role in SST variability by affecting the depth of the upper ocean mixed layer. Even the mean seasonal cycle of mixed layer depth can induce winter-to-winter memory or persistence of SST anomalies via the "re-emergence" mechanism (Namias and Born, 1974; Alexander and Deser., 1995; Deser et al., 2003). Several of these processes have been incorporated to extend the framework of the stochastic climate model, including the "re-emergence" mechanism (Deser et al., 2003) and horizontal advection (Frankignoul and Reynolds, 1983; DeCoetlogon and Frankignoul, 2003).

3. SST Data Sets

The patterns of variability sampled in any particular SST data set will depend to some extent on the spatial and temporal resolution of the data and the length of record. For example, satellite-based SST archives of high spatial resolution but short duration

may reveal patterns with enhanced meso-scale definition but lack information on multi-decadal variability. Conversely, historical ship-based archives of coarse and uneven spatial sampling but long duration may reveal patterns with time scales of multiple decades and longer but lack detailed spatial information. Here we provide a brief overview of the most commonly used SST data sets in climate studies, including information on their spatial resolution and temporal coverage, as well as any filling procedures used to account for missing data. Our discussion will be limited to those data sets that are available on a regular grid over the world oceans (Table 1).

The International Comprehensive Atmosphere-Ocean Data Set (ICOADS) is an extensive and widely used digital collection of quality-controlled surface weather observations (including SST). The majority of the measurements come from ships-of-opportunity, supplemented in recent years by research vessels, moored environmental buoys, drifting buoys, and near-surface measurements from hydrographic profiles. The data are monthly averaged and binned into 2º latitude by 2º longitude boxes beginning in 1800 (1º by 1º beginning in 1960) and extending through 2007 with updates every few years.

Due to the uneven distribution of commercial shipping routes and changes in those routes over time, data coverage is poor in certain regions and periods (Figure 3). Broadly speaking, the North Atlantic, western South Atlantic and northern Indian Oceans contain the highest density of observations, with reasonable coverage back to about 1870. Data coverage is limited in the North Pacific before about 1946 and in the Tropics before about 1960; the Southern Oceans remain poorly sampled throughout the record. The

uneven and changing spatial coverage of SST measurements from historical ship-based archives must be taken into account in any analyses.

Individual SST measurements in the ICOADS are subjected to quality-control procedures to remove outliers and duplicates. However, the screened values are not corrected for changes in instrumentation, observing practice, ship type, etc; missing grid boxes are not filled in; and no "analysis" of the data is performed (e.g., no spatial or temporal smoothing or interpolation). An example of errors introduced by changes in instrumentation is the spurious warming trend around 1941 as a result of switching from bucket to engine-intake measurements (Thompson et al., 2008). The lack of spatial and temporal smoothing in the ICOADS, along with large uncertainties in individual monthly mean values due to inadequate sampling, makes it difficult to produce comprehensible maps of a particular climatic variable for a specific month and year without additional processing of the data.

Various empirical and statistically optimal procedures have been employed to improve upon the sampling uncertainties, temporal inhomogeneities and missing data in the ICOADS and related archives. These globally-complete monthly SST analysis products (e.g., HadISST, Kaplan, and NCDC in Table 1) are tremendously useful for certain applications, for example in studies of global SST variability and as lower boundary conditions in atmospheric model simulations, although they remain constrained by the quality, quantity and distribution of the original measurements (c.f., Hurrell and Trenberth, 1999). The HadISST data are reconstructed using a two-stage reduced-space optimal interpolation procedure, followed by superposition of quality-improved gridded observations onto the reconstructions to restore local detail (Rayner et al., 2003). Similar

methods are used for Kaplan and NCDC (see web addresses in Table 1 for detailed information). In this review, we make use of the HadISST data set in part because of the higher spatial resolution (1º latitude by 1º longitude) compared to the Kaplan (5º latitude by 5º longitude) and NCDC (2º latitude by 2º longitude) archives.

With the advent of satellite retrievals of SST beginning in the early 1980s, there is now full SST coverage over the world oceans at high temporal (every few days) and spatial (~ 10 – 25 km) resolution. Various satellite retrieval methods are available, including infrared sensors from the Advanced Very High Resolution Radiometer (AVHRR) and microwave measurements from the Advanced Microwave Scanning Radiometer (AMSR). The satellite data have also been blended with conventional in-situ data to account for biases and inhomogenieties associated with changing satellites and orbits through time (NOAA Optimum Interpolation products: see Table 1).

4. Geographical Patterns of non-seasonal SST variability

a. Standard Deviations

A common approach to quantifying the magnitude and spatial distribution of non-seasonal SST variability is to map the standard deviation (σ) of the monthly SST anomalies (defined as the departure of the SST for a particular month from the long-term monthly mean) at each location. Figure 4 (lower panel) shows the σ distribution based on satellite-derived SST values during 1982-2008. The long-term mean SST distribution is also shown for reference (Figure 4, top panel). Three regions stand out as having the largest non-seasonal variability: the upwelling zones along the equatorial Pacific and coastal Peru; the western boundary current regions of the Kuroshio and Gulf Stream; and

the Southern Ocean from the tip of South Africa eastward into the Indian Ocean. Maximum values of the SST anomaly standard deviations in these regions exceed 1.5º C. In the extra-tropics, the regions of maximum SST anomaly standard deviation coincide with regions of maximum north-south mean SST gradients (termed "frontal zones"). In the tropics, the highest standard deviations occur where there is a local minimum in the long-term mean SSTs due to equatorial and coastal upwelling. Apart from the regions of maximum SST anomaly standard deviation, there is relatively high variability (standard deviations around 0.75ºC - 1ºC) across the North Pacific and North Atlantic and the South Pacific, South Indian, and South Atlantic and relatively low variability across the Tropical ocean basins (standard deviations around 0.3ºC – 0.5ºC). A similar map based on the COADS archive lacks the sharpness of the SST variance maxima seen in the satellite data due to the coarser sampling in both space and time.

b. Methods for identifying patterns of variability

The standard deviation map of non-seasonal SST anomalies presented in Figure 4 does not give any information on how SST variations at one location are related to those at another. To ascertain the co-variability of SST anomalies at different locations, alternative analysis methods are needed. One commonly used approach is Empirical Orthogonal Function (EOF) analysis and extensions thereof (von Storch and Zwiers, 1999). Conceptually, EOF analysis determines a spatio-temporal pattern of variability that accounts for the maximum co-variance between the SST anomaly time series at all pairs of grid points in the data set. Then, the remaining co-variability is subject to the same decomposition with the added constraint that the 2nd spatio-temporal EOF pattern is

orthogonal (e.g., uncorrelated) in both time and space to the leading EOF pattern. This procedure is repeated until all *n* EOF patterns have been computed, where *n* is equal to the number of grid points. In practice, only the first few leading modes are robust due to the orthogonality constraint. EOF rotation may be used to circumvent this constraint; however, it may also result in patterns that are overly-localized in space. Each EOF pattern is associated with a principal component (PC) time series which describes the temporal evolution of the EOF pattern. The PC time series may be obtained by projecting the EOF pattern onto the original SST anomaly field at each time step so as to find the sign and amplitude of the pattern at any given time. It should be noted that the sign of the EOF is arbitrary; however, the product of the EOF and the PC time series recovers the correct polarity of the mode at any given grid box and time.

Although useful, EOF analysis is not fool-proof. The EOF modes depend on the spatial domain considered, are subject to orthogonality constraints, and may not be separable if they account for similar percentages of the total variance (North et al., 1982). Also, EOFs are empirically determined "modes" and thus are not necessarily equivalent to the dynamical modes of the system. It is always prudent to confirm EOF patterns with simpler techniques such as compositing, one-point correlation maps, and linear regression analysis. Some examples are given in the next section.

5. Dominant patterns of non-seasonal SST variability

a. Tropics

i. ENSO

The leading EOF of monthly SST anomalies over the globe is the ENSO mode. Here we show the leading EOF based on linearly detrended monthly anomalies during the period 1900-2008 from the HadISST data set (Figure 5a), but similar results are found for shorter time periods and other SST data sets. This single mode accounts for 19% of the non-seasonal variability of SSTs over the global oceans during the past 109 years. The spatial pattern associated with the warm phase of ENSO consists of positive SST anomalies across the eastern two-thirds of the equatorial Pacific Ocean, flanked by weaker negative anomalies over the far western tropical Pacific and extending in a horseshoe-like fashion to the North and South Pacific; positive SST anomalies are also found along the west coasts of North and South America. ENSO-related SST anomalies also occur over the Atlantic, Indian, and Southern Oceans.

A commonly used index for representing SST variability associated with ENSO is the area average of monthly SST anomalies in the region 5°N–5°S, 170°–120°W (outlined by the box in Figure 5a), and is referred to as the "Niño-3.4 SST index" for historical reasons having to do with the configuration of ship tracks in the region (Rasmusson and Carpenter, 1982). The Niño-3.4 SST index is nearly identical to the principal component time series associated with the leading EOF: their correlation coefficient is 0.93. The Niño-3.4 time series exhibits an irregular series of warm and cold "events" typically lasting about 1–1.5 yr and recurring approximately every 3–8 yr (Figure 5b). The largest warm events such as those that occurred in 1982-83 and 1997-98 have amplitudes of approximately 2º - 2.5º C, while more moderate warm events range from 1º C to 2º C. Cold events tend to be somewhat weaker and longer lasting than their warm counterparts. A power spectrum of the Niño-3.4 time series shows that the

dominant range of periods is 2.5–8 years, with some sensitivity to the period of record sampled (Figure 5c). ENSO is seasonally dependent as indicated by the seasonal cycle of the standard deviation of the Niño-3.4 SST anomaly time series (Figure 5d) which shows minimum values (~ 0.55º C) during April–June and maximum values (~ 0.95º C) near the end of the calendar year (November–January).

ENSO-related SST anomalies evolve substantially during the course of a warm or cold event. A composite ENSO evolution over a period of 6 seasons is shown in Figure 6, starting with conditions during March-May before the peak and ending with conditions in June-August of the following year. The warm event composite is based on selecting the years for which the Niño-3.4 SST index in September-November exceeds 1 standard deviation based on the period 1950-2008; similarly, the cold event composite is based on selecting the years for which the September-November Niño-3.4 SST index is less than -1 standard deviation. The cold event composite is then subtracted from the warm event composite. The composite ENSO evolution is depicted for linearly detrended SST and SLP anomalies in Figure 6. Note that this approach is independent of the EOF analysis shown earlier.

The ENSO composite SST evolution exhibits an incipient warming along the equator and coast of South America during MAM0 that subsequently grows in amplitude over the next several seasons, reaching its peak around SON0 and DJF1. [Here, the first year of the ENSO event is denoted by a “0” and the subsequent year by a “1”.] The warm event diminishes during MAM1 and begins to transition to a weak cold event in JJA1. Accompanying the warming is the simultaneous development of negative SST anomalies in the northwest and southwest tropical Pacific. The tropical Indian Ocean as well as

portions of the tropical Atlantic exhibits a delayed warming relative to that in the Pacific, reaching peak strength around DJF1 and MAM1 but lingering through JJA1 and beyond. Similar results are shown in Harrison and Larkin (1998), Rasmusson and Carpenter (1982), Trenberth et al. (2002), and Klein et al. (1999), among others. Tropical SLP anomalies develop in tandem with the SST anomalies, reaching maximum strength in DJF1. This large-scale SLP anomaly pattern, with positive values west of the International Date Line and negative values to the east, is associated with the negative phase of the Southern Oscillation (see also Deser and Wallace, 1990; Harrison and Larkin, 1996).

Not all ENSO events follow the canonical evolution depicted in Figure 6. For example, some events develop mainly in the central equatorial Pacific while others are confined to the coast of South America (Deser and Wallace, 1987; Kao and Yu; 2009). In addition, some events show an eastward spreading of the equatorial Pacific SST anomalies (Guan and Nigam, 2008) in contrast to the westward development of the composite ENSO.

ENSO is understood to be a natural mode of variability of the coupled ocean-atmosphere system in the tropical Pacific. Over the past 25 years, two broad paradigms have emerged to explain the governing dynamics of ENSO. One paradigm is the "delayed oscillator" or "recharge oscillator" theory which holds that ENSO is an unstable mode of the coupled tropical ocean-atmosphere system exhibiting self-sustained, regular oscillations (Zebiak and Cane, 1987; Battisti, 1988; Schopf and Suarez, 1998). Irregularity in the ENSO period can occur through stochastic forcing (noise) in the form of energetic weather events such as the Madden-and-Julian Oscillation and westerly wind

bursts or through low-order chaos (Munnich et al., 1991; Jin et al., 1994; Blanke et al., 1997). The other leading paradigm is the stochastic forcing theory which holds that ENSO is a damped stable mode of the system which requires energy from stochastic forcing to maintain the oscillation (Penland and Sardeshmukh, 1995; Chang et al., 1996; Moore and Kleeman, 1999; Thompson and Battisti, 2001). Regardless of the precise nature of the ENSO mode, a series of positive and negative feedbacks between the atmosphere and ocean within the tropical Pacific lead to the growth and decay of an event. The dominant positive feedback is the so-called "Bjerknes Feedback" between the wind anomalies in the western and central equatorial Pacific and the SST anomalies in the eastern Pacific. According to the Bjerknes feedback mechanism, westerly wind anomalies produce positive SST anomalies through downwelling equatorial oceanic Kelvin waves, and these SST anomalies in turn weaken the zonal SLP gradient which leads to westerly wind anomalies. The dominant negative feedback involves the dynamical adjustment of the equatorial Pacific thermocline to the overlying wind field with a time delay that eventually leads to the demise of an event. Much progress has been made on the predictability of ENSO, leading to the routine issuance of ENSO forecasts (e.g., Palmer et al. 2004).

ii. ENSO teleconnections: The Atmospheric Bridge

While air-sea interactions responsible for ENSO are centered over the equatorial Pacific Ocean, changes in tropical precipitation from deep convection associated with ENSO influence the global atmospheric circulation, in part through the excitation of Rossby waves that emanate into the extratropics of both hemispheres. The wave energy

tends follows great circle routes, initially extending poleward and eastward, refracting (turning) away from the pole and returning to the tropics. These planetary waves form in preferred locations, which include high pressure in the subtropics and low pressure in midlatitudes of the North and South Pacific. The overall structure of the ENSO response is influenced by additional factors, including the detailed structure of the climatological wind field that governs the path of the wave energy, sources/sinks of Rossby waves outside of the tropical Pacific and changes in the storm tracks (see reviews by Trenberth et al., 1998; Liu and Alexander 2007). The ENSO-driven circulation patterns alter the near-surface air temperature, humidity and wind, as well as the distribution of clouds far from the equatorial Pacific. The resulting variations in the surface heat, momentum, and freshwater fluxes induce changes in SST as well as salinity, mixed layer depth, and ocean currents. Thus, the atmosphere acts as a bridge spanning from the equatorial Pacific to the remainder of the global oceans.

Atmospheric teleconnections to the North Pacific peak during DJF1, manifest by large amplitude negative SLP anomalies centered over the Gulf of Alaska (Figure 6). This pattern, the surface expression of the PNA, results in anomalous northwesterly winds that advect relatively cold dry air over the western/central North Pacific, anomalous southerly winds that advect warm moist air along the west coast of North America and enhanced surface westerlies over the central North Pacific. The resulting anomalous surface heat fluxes and Ekman transport create negative SST anomalies in the central and western North Pacific and positive SST anomalies along the west coast of North America (Alexander et al., 2002).

The wintertime ENSO response also impacts the North Atlantic (Figure 6). During El Niño events, a pattern similar but not identical to the NAO develops in DJF1, with anomalous high (low) pressure in high (mid) latitudes in conjunction with a southward displacement and intensification of the storm track along the eastern seaboard. This change in the atmospheric circulation creates a large-scale pattern of SST anomalies through the mechanisms discussed previously in Section 2. The SST response most closely resembles the tri-pole pattern in MAM1, with negative anomalies in mid latitudes flanked by positive anomalies in the subarctic and subtropics. Observational studies and model experiments suggest that the ENSO teleconnection over the North Atlantic is stronger and more robust during La Niña events compared to El Niño events (Pozo-Vazquez et al., 2001).

ENSO-driven atmospheric teleconnections to the Southern Hemisphere are in many ways symmetric to those in the Northern Hemisphere (Figure 6). For example, negative SLP anomalies develop over the South Pacific in austral winter (JJA0), in analogy with those over the North Pacific in boreal winter (DJF1). During austral summer (DJF1), the remote response to ENSO includes not only a wavelike response but also a component that projects onto the Southern Annular Mode (SAM), with negative SLP anomalies over middle latitudes and positive SLP anomalies over high latitudes. The Southern Hemisphere SST response to these atmospheric circulation anomalies include negative anomalies at ~30°S and positive anomalies near the Antarctic Peninsula during El Niño events. These SST anomalies are primarily driven by surface heat fluxes in midlatitudes and Ekman transport in high latitudes in both summer and winter (Ciasto and Thompson, 2008). The amplitude of the SST anomalies is largest during austral

summer, when the mixed layer is shallow and thus the ocean can rapidly respond to thermal forcing.

As mentioned earlier, the tropical Indian Ocean warms following an El Niño event, with SST anomalies that lag those in the central Pacific by about 3-6 months. Part of the basin-wide warming is generated by the diminished wind speeds which reduce the upward latent heat flux and by the reduced cloudiness which allows more solar radiation to reach the surface (Klein et al., 1999). Ocean dynamics also influences El Niño-related SST anomalies in parts of the Indian Ocean: westward propagating oceanic Rossby waves generated by anomalous wind stress curl in the southern Indian Ocean contribute by depressing the relatively shallow thermocline at ~10°S (Xie et al., 2002). The slow propagation of the oceanic Rossby waves maintains the Indian Ocean SST anomalies through JJA1, with associated atmospheric teleconnections to the subtropical Northwest Pacific and East Asia (Xie et al. 2009).

iii. Non-ENSO variability in the Tropical Indian and Atlantic Oceans

a. Tropical Indian Ocean Dipole

The two leading EOFs of detrended monthly SST anomalies over the tropical Indian Ocean (20^oN - 20^oS) are the basin-wide mode and the east-west dipole mode, respectively (Figure 7). The former is closely linked to ENSO as described in the previous section, while the latter occurs both in conjunction with and independently of ENSO. The two modes differ not only in their spatial expression, but also in their seasonal dependence: the basin-wide mode peaks in January-March while the dipole mode peaks in July-October (Figure 7). The positive phase of the dipole mode exhibits

weak positive SST anomalies over the western two-thirds of the basin and strong negative SST anomalies in the vicinity of Indonesia. A positive dipole mode is evident in the ENSO composite during SON0 (Figure 6).

Bjerknes feedback appears to contribute to the development of the dipole mode: the eastern cooling induces easterly wind anomalies which in turn drive equatorial upwelling which shoals the thermocline, thereby reinforcing the SST cooling (Saji et al. 1999). The east-west seesaw in the thermocline depth is part of the transient adjustment in response to wind variability near the equator. In fact, the dipole mode stands out as the leading mode in EOF analysis of thermocline depth variability (Shinoda et al. 2004). The SST dipole mode is strongest during July-November when upwelling-favorable southeasterly alongshore winds prevail off the coast of Indonesia, and it is linked to a similar dipole in precipitation (negative in the east and positive in the west during the positive phase). See Schott et al. (2009) for a recent review of Indian Ocean climate variability. Predictability of the Indian Ocean dipole mode is discussed in Luo et al. (2007).

b. Tropical Atlantic

There are two major modes of tropical Atlantic variability: an equatorial mode akin to the Pacific El Niño, and a meridional mode characterized by cross-equatorial SST anomaly gradients (a similar mode is also found in the tropical Pacific). Recent reviews of these modes are provided in Xie and Carton (2004) and Chang et al. (2006).

Atlantic Niño

The equatorial Atlantic cold tongue displays significant year-to-year variability, with typical amplitude ~ 0.5 ^{o}C and frequency ~ 2-3 years. This equatorial mode, called the Atlantic Niño, appears as the leading mode of tropical Atlantic variability with strongest amplitude during May-July (Fig. 8). It is similar to ENSO in that ocean-atmospheric interactions give rise to positive feedbacks similar to those envisioned by Bjerknes for ENSO in the Pacific. The anomalous warming in the eastern equatorial Atlantic relaxes the easterly Trade winds, which reinforce the eastern warming by weakening the equatorial upwelling and lowering the thermocline (Zebiak 1993). The Atlantic Niño intensifies atmospheric convection near the equator, and keeps the summer rain band from advancing into the Sahel while increasing rainfall at the Gulf of Guinea coast (Giannini et al. 2003). The Atlantic Niño is weaker and higher in frequency than its Pacific counterpart.

Meridional mode

The second EOF mode of tropical Atlantic SST variability shows a meridional dipole pattern with the nodal line displaced slightly north of the equator (Fig. 8). The warm (cool) pole is associated with the relaxed (intensified) easterly trades (Nobre and Shukla 1996). Such a wind-SST relation suggests the following positive feedback *via* surface evaporation (Chang et al. 1997). An initial SST dipole induces southerly winds across the equator. The Coriolis force causes these southerlies to gain a westerly (easterly) component in the warm (cool) hemisphere, decelerating (accelerating) the prevailing easterly trades. The resultant changes in surface evaporation act to amplify the initial SST dipole. This wind-evaporation-SST (WES) feedback preferentially amplifies

equatorial-antisymmetric disturbances while the Bjerknes feedback grows east-west variations on the equator. A similar phenomenon exists in the Pacific (Chiang and Vimont, 2004), with growing evidence that it may play an important role in initiating ENSO events (Chang et al., 2007).

The meridional mode is most pronounced during the equatorial warm season March-May, with SST anomalies typically ~ 0.5^{o}C in the subtropics. The attendant SST gradients across the equator are very effective in displacing the Atlantic Inter-tropical Convergence Zone (ITCZ) into the warmer hemisphere. Rainfall in the semi-arid Nordeste region of Brazil is sensitive to this meridional mode and the ITCZ shifts it induces (Nobre and Shukla 1996). The meridional mode also affects North Atlantic hurricanes through its influence on SST in the main development region (90-20^{o}W, 5-25^{o}N) (Wang et al. 2006; Vimont and Kossin 2007).

Besides WES feedback, there are several other factors for variability in the cross-equatorial SST gradient. For example, ENSO affects SSTs over the tropical North Atlantic (recall Fig. 6), while the North Atlantic Oscillation forces the same region by changing the northeast Trade winds (recall Figure 1; see also Xie and Tanimoto 1998; Czaja et al. 2002). These and other factors result in a weak correlation between subtropical SST anomalies north and south of the equator. It has been suggested that the North Atlantic tripole (Deser and Blackmon 1993) and a South Atlantic dipole (Venegas et al. 1997) are correlated to form a pan-Atlantic pattern through the coordination of WES feedback across the equator (Xie and Tanimoto 1998).

a. Extra-tropics

i. Southern Hemisphere

Given the paucity of SST measurements from ships-of-opportunity, studies of SST variability in the Southern Hemisphere rely mainly on satellite-based data sets. The leading EOF pattern of SST anomalies south of 20°S from the NOAA OI SST data set for the period 1981-2005 from Ciasto and Thompson (2008) is reproduced in Figure 9. This analysis was performed separately for the warm season, November-April, and the cold season, May-October. Superimposed upon the SST EOF patterns are the associated 500 hPa geopotential height anomaly patterns, obtained by regressing seasonal anomalies at each grid box upon the SST PC time series. Similar patterns are obtained for SLP (not shown). In both seasons, the leading EOF (in its positive polarity) exhibits positive SST anomalies across much of the South Pacific and negative SST anomalies in the Pacific sector of the Southern Ocean. The warm season pattern also exhibits positive SST anomalies across the Indian and Atlantic sectors of the Southern Ocean, with negative anomalies to the north and adjacent to the coast of Antarctica.

As Ciasto and Thompson (2008) demonstrate, the SST anomalies associated with the leading mode of variability are largely atmospherically forced via changes in the surface turbulent fluxes and to a lesser extent Ekman currents. The associated 500 hPa geopotential height anomaly pattern resembles that due to ENSO (recall Figure 6), with an additional component related to the Southern Annular Mode (SAM) during the warm season. Although the SST anomalies depicted in Figure 9 are primarily forced by the atmosphere, there is evidence for a back effect onto the atmosphere, manifest as an increase in the persistence time for the SAM above that due to intrinsic atmospheric dynamical processes (Sen Gupta and England, 2007).

ii. Pacific Decadal Oscillation

The leading EOF of monthly SST anomalies over the North Pacific (after removing the global mean SST anomaly) and its associated PC time series are termed the Pacific Decadal Oscillation (PDO) after Mantua et al. (1997). This mode, which accounts for 25% of the variance of monthly anomalies in the HadISST data set during the period 1900-2008, is displayed in Figure 10. Although the EOF calculation was restricted to the North Pacific (20° N - 70° N), the pattern is displayed globally by regressing the monthly SST anomalies at each location upon the PC time series. The spatial pattern of SST anomalies associated with the PDO is similar to that associated with ENSO (recall Figure 6) except for the relative weighting between the north and tropical Pacific. In particular, the amplitudes of the SST anomalies in the equatorial eastern Pacific compared to those in the North Pacific are comparable for the PDO whereas they are considerably larger for ENSO (see also Zhang et al., 1997; Garreaud and Battisti, 1999; Dettinger et al., 2000; Deser et al., 2004). The PDO has also been termed the Interdecadal Pacific Oscillation (IPO; Power et al., 1999) in recognition of its extension to the South Pacific.

The time series of the PDO exhibits considerable decadal variability, hence its name (Figure 10, bottom). Even the raw monthly anomalies show periods of predominantly one sign lasting for two decades or longer (for example, the periods 1908-1945, 1947-1976 and 1977-1998). The decadal SST transitions are accompanied by widespread changes in the atmosphere, ocean and marine ecosystems. For example, Mantua et al. (1997) found that the timing of changes in the PDO closely corresponded to those in salmon catch along the west coast of North America. The Aleutian Low pressure system also fluctuates

in tandem with the PDO SST variations (Deser et al, 2004). Given the relatively short observational record, it is difficult to ascertain whether there is a robust spectral peak in the PDO time series. Some studies suggest nominal time scales of ~ 20 years and ~ 50 years (Minobe, 1997; Minobe, 1999; Deser et al., 2004) while others conclude that the PDO record does not differ significantly from a first-order autoregressive process (e.g., red noise: Pierce, 2001; Qiu et al., 2007).

Many different mechanisms have been proposed for the PDO, including random forcing of the ocean by the atmosphere according to the stochastic climate model paradigm (recall Section 2), the atmospheric bridge from the tropical Indo-Pacific, extratropical ocean processes, and atmosphere-ocean interactions within the North Pacific (see the recent review in Alexander, 2009). How can we reconcile these different mechanisms for the PDO? Several studies have used statistical analyses to reconstruct the PDO and determine the processes that underlie its dynamics (Newman et al, 2003; Vimont, 2005; Schneider and Cornuelle, 2005; Qiu et al., 2007; Newman, 2007). Taken together, theses studies indicate that on interannual time scales, random and ENSO-induced fluctuations in the strength of the Aleutian Low are about equally important in determining PDO variability via surface heat flux forcing, with negligible contribution from ocean currents. On decadal timescales, stochastic heat flux forcing, the atmospheric bridge, and changes in the North Pacific oceanic gyre circulation contribute approximately equally. Over the western Pacific east of Japan where a deep mixed layer develops during winter, ocean circulation changes associated with latitudinal excursions of the Kuroshio Current Extension are of primary importance for PDO-related SST variability (Nonaka et al. 2006; Taguchi et al. 2007). A key implication of these analyses

is that, unlike ENSO, the PDO is likely not a single physical mode but rather the sum of several phenomena.

The PDO is only one measure of SST variability in the North Pacific. Other recurring patterns include the "North Pacific" mode (Deser and Blackmon, 1995; Nakamura et al., 1997; Barlow et al., 2001; Guan and Nigam, 2008) which is closely related to the PDO albeit with less amplitude in the tropical Indo-Pacific. A distinct "Pan-Pacific mode" has also been identified which emphasizes variability in the eastern portion of the North Pacific (Guan and Nigam, 2008), and a "North Pacific Gyre Oscillation" mode which is also evident in sea surface height variability (Di Lorenzo et al., 2007). The mechanisms governing these modes are not well understood.

iii. Atlantic Multi-decadal Oscillation

SSTs in the North Atlantic undergo slow variations with a period on the order of 65-80 years (Kushnir, 1994; Schlesinger and Ramankutty, 1994; Delworth and Mann, 2000; Enfield et al., 2001; Ting et al., 2009; Guan and Nigam, 2009). This phenomenon has been termed the Atlantic Multi-decadal Oscillation (AMO; Kerr, 2000). A simple index of the AMO is shown in Figure 11 for the period 1870-2008 based on the HadISST data set (note that SST observations are relatively plentiful in the North Atlantic back to 1870; recall Figure 3). This index is defined as the area-average SST anomaly over the North Atlantic (0°-70°N) minus the global mean SST anomaly. Warm phases occurred from the late 1920s through the late 1960s and since the mid-1990s, and cool phases occurred from the early 1900s through the mid-1920s and from the early 1970s through the mid-1990s. The spatial pattern associated with this time series, obtained by linearly

regressing the SST anomalies at each location upon the AMO index, exhibits positive values over the entire North Atlantic, with the largest magnitudes (approximately 0.5ºC) south of Greenland.

The AMO is associated with large-scale precipitation changes, most notably over the Sahel, the southeastern United States and Brazil (Enfield et al., 2001; Ting et al., 2009), and with the frequency of severe Atlantic hurricanes (Enfield et al., 2001). It should be noted that the AMO is not significantly correlated with the NAO (Guan and Nigam, 2009). The precise nature of the AMO is still being refined and clarified. In particular, the role of Pacific SST variability is not well understood. For example, Ting et al. (2009; see also Enfield et al., 2001) show some connection between the AMO and SST anomalies in the Gulf of Alaska and the tropical Pacific (see also Figure 11), while the analysis of Guan and Nigam (2009) indicates that there are no significant SST linkages outside of the North Atlantic.

The AMO is considered to be a natural mode of oscillation of the Atlantic Ocean's thermohaline circulation (Delworth and Mann, 2000). Modeling studies indicate that this mode is intrinsic to the ocean and stochastically forced by atmospheric buoyancy fluxes (Delworth and Greatbatch, 2000). However, the amplitude of the mode is augmented due to coupled ocean-atmosphere interactions.

There has been considerable debate concerning the degree to which anthropogenic effects may be contributing to the recent positive phase of the AMO. In particular, there has been a general warming trend over both land and ocean associated with increasing greenhouse gas concentrations. Since the AMO index is a temperature-based record, it may contain the anthropogenic global warming signal and thus partially confound the

true state of the AMO. There have been various attempts to remove the anthropogenic global warming signal from the AMO index, including simple linear detrending, removal of the global mean temperature anomaly (as in Figure 1), and removal of model-based estimates of the forced component of variability. The latter approach has been shown to provide the best estimate of the natural component of the AMO (Ting et al., 2009). This natural component, shown by the green curve in Figure 11, indicates that the AMO is currently in a modest warm phase, not an extreme warm phase as would be inferred from the raw SST index (Ting et al., 2009; Guan and Nigam, 2009). It should be noted that the Atlantic thermohaline circulation may itself be altered under anthropogenic forcing as projected by some climate models (Dixon et al., 1999; Wood et al., 1999) but this issue is distinct from that of the overall global warming trend in the temperature-based AMO index.

6. Summary Points

1) Interannual and longer time scale SST variations exhibit large-scale organization due to both atmospheric and oceanic processes.

2) Such large-scale organization may be due to intrinsic modes of atmospheric circulation variability which imprint themselves upon the SST field mainly via surface energy fluxes but also Ekman currents. Examples include: SST fluctuations in the Southern Ocean associated with the Southern Annular Mode; a tri-polar pattern of SST anomalies in the North Atlantic associated with the North Atlantic Oscillation; and a pan-Pacific mode known as the Pacific Decadal Oscillation. Oceanic processes also contribute to the latter.

3) A leading paradigm for these atmospherically-forced patterns of SST variability is the stochastic climate model whereby random fluctuations in the atmospheric circulation give rise to a low-frequency SST response.

4) Patterns of non-seasonal SST variability may also result from coupled ocean-atmosphere interactions, most prominently the El Niño/Southern Oscillation phenomenon in the tropical Indo-Pacific sector, but also the tropical Atlantic Niño and the cross-equatorial meridional modes of the tropical Pacific and Atlantic.

5) Intrinsic oceanic modes also may give rise to large-scale patterns of SST variability. A leading example is the Atlantic Multidecadal Oscillation associated with changes in the oceanic thermohaline circulation.

7. Future Issues

A number of outstanding issues remain regarding the patterns and mechanisms of non-seasonal SST variability, exemplified in the following questions.

1) Does the response to global warming (e.g., increasing greenhouse gas concentrations) project onto known patterns of natural SST variability, or does it create new patterns?

2) How much does feedback from the ocean to the atmosphere influence the atmospherically-driven modes of extra-tropical SST variability?

3) What is the nature of the predictability of the tropical and extra-tropical modes of SST variability on decadal time scales?

4) What are the linkages among the different natural modes of SST variability, and what mechanisms produce these connections?

5) Do high resolution satellite data sets reveal new patterns of SST variability?

6) Do empirical methods such as EOF analysis identify the true physical modes of SST variability?

7) How do the patterns of SST variability relate to those in the ocean interior?

Acknowledgments

Support from the NOAA Climate Program Office's Climate Variability and Predictability Program is gratefully acknowledged. The National Center for Atmospheric Research is supported by the National Science Foundation.

References

Alexander MA. 2008. Extratropical Air-Sea Interaction, SST Variability and the Pacific Decadal Oscillation (PDO). In *Climate Dynamics: Why does Climate Vary,* ed D Sun and F Bryan, AGU Monograph: Submitted

Alexander, MA, Bladé I, Newman M, Lanzante JR, Lau N-C, Scott JD. 2002. The atmospheric bridge: The influence of ENSO teleconnections on air–sea interaction over the global oceans. *J. Climate*. 15:2205-31

Alexander MA, Deser C. 1995. A mechanism for the recurrence of wintertime midlatitude SST anomalies. *J. Phys. Oceanogr*. 122-37

Alexander MA, Scott JD 1997. Surface flux variability over the North Pacific and North Atlantic Oceans. *J. Climate*. 10:2963-78

Alexander MA, Scott JD. 2008. The role of Ekman ocean heat transport in the Northern Hemisphere response to ENSO. *J. Climate*. 21:5688-707

Barlow M, Nigam S, Berbery EH. 2001. ENSO, Pacific Decadal Variability, and U.S. Summertime Precipitation, Drought, and Stream Flow. *J. Climate*. 14:2105-28

Barnston G, Livezey RE. 1987. Classification, seasonality and low-frequency atmospheric circulation patterns. *Mon. Wea. Rev*. 1083-126

Battisti DS. 1988. Dynamics and thermodynamics of a warming event in a coupled tropical at mosphere-ocean model. *J. Atmos. Sci.* 45:2889-919

Blanke B, Neelin JD, Gutzler D. 1997. Estimating the effect of stochastic wind stress forcing on ENSO irregularity. *J. Climate*. 10:1473-86

Cayan DR. 1992. Latent and sensible heat flux anomalies over the northern oceans: driving the sea surface temperature. *J. Phys. Oceanogr.* 22:859-81

Chang P, Ji L, Li H. 1997. A decadal climate variation in the tropical Atlantic ocean from thermodynamic air-sea interactions. *Nature*. 385:516-18

Chang P, Ji L, Li H, Flügel M. 1996. Chaotic Dynamics versus stochastic processes in El Niño-Southern Oscillation in coupled ocean-atmosphere models. *Physica D*. 98:301-20

Chang P, Yamagata T, Schopf P, Behera SK, Carton JA, et al. 2006. Climate fluctuations of tropical coupled system: The role of ocean dynamics. *J. Climate*. 19:5122–74

Chang P, Zhang L, Saravanan R, Vimont DJ, Chiang JCH, et al. 2007. Pacific meridional mode and El Niño-Southern Oscillation. *Geophys. Res. Lett*. 34:L16608, doi:10.1029/2007GL030302

Chiang JC, Vimont DJ. 2004. Analogous Pacific and Atlantic meridional modes of tropical atmosphere-ocean variability. *J. Climate*. 17:4143-58

Ciasto LM, Thompson DWJ. 2008. Observations of Large-Scale Ocean–Atmosphere Interaction in the Southern Hemisphere. *J. Climate*. 21:1244–1259

Czaja A, Frankignoul C. 2002. Observed impact of Atlantic SST anomalies on the North Atlantic Oscillation. *J. Climate*. 15:606-23

Czaja A, van der Vaart P, Marshall J. 2002. A diagnostic study of the role of remote forcing in tropical Atlantic variability. *J. Climate*. 15:3280-90

de Coëtlogon G, Frankignoul C. 2003. On the persistence of winter sea surface temperature in the North Atlantic. *J. Climate*. 16:1364-77.

Delworth T, Greatbatch RJ. 2000. Multidecadal thermohaline circulation variability driven by atmospheric surface flux forcing. *J. Climate*. 13:1481-95

Delworth T, Mann ME. 2000. Observed and simulated multidecadal variability in the Northern Hemisphere. *Climate Dyn.* 16:661-76

Deser C, Alexander MA, Timlin MS. 2003. Understanding the persistence of sea surface temperature anomalies in midlatitudes. *J. Climate*. 16:57-72

Deser C, Blackmon ML. 1993. Surface Climate Variations over the North Atlantic Ocean during Winter: 1900-1989. *J. Climate*. 6:1743-53

Deser C, Blackmon ML. 1995: On the Relationship between Tropical and North Pacific Sea Surface Temperature Variations. *J. Climate*. 8:1677-80

Deser C, Phillips AS. 2006. Simulation of the 1976/1977 Climate Transition over the North Pacific: Sensitivity to Tropical Forcing. *J. Climate*. 19:6170-80.

Deser C, Phillips AS, Hurrell JW. 2004. Pacific interdecadal climate variability: Linkages between the Tropics and the North Pacific during boreal winter since 1900. J. *Climate*. 17:3109-24

Deser C, Timlin MS. 1997. Atmosphere-ocean interaction on weekly timescales in the North Atlantic and Pacific. *J. Climate*. 10:393-408

Deser C, Wallace JM. 1987. El Nino events and their relationship to the Southern Oscillation: 1925-1986. *J. of Geophys. Res*. 92:14189-96

Deser C, Wallace JM. 1990. Large-scale atmospheric circulation features of war m and cold episodes in the tropical Pacific. *J. Climate*. 3:1254-81

Dettinger MD, Cayan DR, McCabe GM, Marengo JA. 2000. Multiscale streamflow variability associated with El Nino/Southern Oscillation. In *El Nino and the Southern Oscillation--Multiscale Variability and Global and Regional Impacts*, ed. HF Diaz, V Markgraf, Cambridge University Press, pp. 113-46

Di Lorenzo E, Schneider N, Cobb KM, Chhak K, Franks PJS, et al. 2008. North Pacific Gyre Oscillation links ocean climate and ecosystem change. *Geophys. Res. Lett.* 35(L08607), doi:10.1029/2007GL032838

Dixon WK, Delworth TL, Spelman MJ, Stouffer RJ. 1999. The influence of transient surface fluxes on North Atlantic overturning in a coupled GCM climate change experiment. *Geophys. Res. Lett.* 26:2749-52

Enfield DB, Mestas-Nunez AM, Trimble PJ. 2001. TheAtlantic multidecadal oscillation and its relation to rainfall river flows in the continental U.S.. *Geophys. Res. Lett*. 28:2077-80

Feldstein SB. 2000. Teleconnections and ENSO: The time scale, power spectra, and climate noise properties. *J. Climate*. 13:4430-40

Frankignoul C, Hasselmann K. 1977. Stochastic climate models. Part 2. Application to sea-surface temperature variability and thermocline variability. *Tellus*. 29:284-305

Frankignoul C, Reynolds RW. 1983. Testing a dynamical model for mid-latitude sea surface temperature anomalies. *J. Phys. Oceanogr*. 13:1131-1145

Garreaud RD, Battisti DS. 1999. Interannual (ENSO) and Interdecadal (ENSO-like) variability in the southern hemisphere tropospheric circulation. *J. Climate*. 12:2113-23

Giannini A, Saravanan R, Chang P. 2003. Oceanic forcing of Sahel rainfall on interannual to interdecadal time scales. *Science*. 302:1027-30

Guan B, Nigam S. 2008. Pacific Sea Surface Temperatures in the Twentieth Century: An evolution-centric analysis of variability and trend. *J. Climate*. 21:2790-809

Guan B, Nigam S. 2009. Analysis of Atlantic SST Variability Factoring Inter-basin Links and the Secular Trend: Clarified Structure of the Atlantic Multidecadal Oscillation. *Journal of Climate*. 22: In press

Harrison D, Larkin NK. 1996. The COADS sea level pressure signal: A near-global El Niño composite and time series view, 1946–1993. *J. Climate*. 9:3025-55

Harrison DE, Larkin NK. 1998. El Niño-Southern Oscillation Sea Surface Temperature and Wind Anomalies, 1946-1993. *Rev. Geophys*. 36:353–99

Hartmann D. 1994. *Global Physical Climatology*. Academic Press, 411 pp. ISBN 0-12-328530-5.

Hurrell JW, Deser C. 2009. North Atlantic climate variability: The role of the North Atlantic Oscillation. *Journal of Marine Systems*. In press. DOI:10.1016/j.jmarsys.2008.11.026

Hurrell J, Kushnir Y, Ottersen G, Visbeck M. 2003. An overview of the North Atlantic Oscillation. In *The North Atlantic Oscillation: Climatic Significance and Environmental Impact*, pp. 1-35. Geophys. Monogr., Vol. 134, Amer. Geophys. Union

Hurrell JW, Trenberth KE. 1999. Global Sea Surface Temperature Analyses: Multiple Problems and Their Implications for Climate Analysis, Modeling, and Reanalysis. *Bull. Amer. Meteor. Soc*. 80:2661-78

Johnson NC, Feldstein S**B**. 2009. The continuum of North Pacific sea level pressure patterns: Intraseasonal, interannual, and interdecadal variability. *J. Climate*: Submitted

Jin F-F, Neelin D, Ghil M. 1994. El Niño on the devil's staircase: annual subharmonic steps to chaos. *Science*. 264:70-2

Karoly DJ. 1989. Southern Hemisphere Circulation Features Associated with El Niño-Southern Oscillation Events. *J. Climate*. 2:1239–52

Kao H-Y, Yu J-Y. 2009. Contrasting Eastern-Pacific and Central-Pacific Types of ENSO. *J. Climate*. 22:615-32

Kerr RA. 2000. A North Atlantic climate pacemaker for the centuries. *Science*. 288:1984-6

Klein SA, Soden BJ, Lau N-C. 1999. Remote sea surface temperature variations during ENSO: Evidence for a tropical atmospheric bridge. *J. Climate*. 12:917-32

Kushnir Y. 1994. Interdecadal variations in North Atlantic sea surface temperature and associated atmospheric conditions. *J. Climate*. 7:141-57

Kushnir Y, Wallace JM. 1989. Low-Frequency Variability in the Northern Hemisphere Winter - Geographical-Distribution, Structure and Time-Scale Dependence. *J. Atmos. Sci*. 46:3122-42

Liu Z, Alexander MA. 2007. Atmospheric Bridge, Oceanic Tunnel and Global Climatic Teleconnections. *Rev. Geophys*. 45, RG2005, doi:2010.1029/2005RG000172

Luo JJ, Masson S, Behera S, Yamagata T. 2007. Experimental forecasts of the Indian Ocean Dipole using a coupled OAGCM. *J. Climate*. 20:2178–90

Mantua NJ, Hare SR, Zhang Y, Wallace JM, Francis R. 1997. A Pacific interdecadal climate oscillation with impacts on salmon production. *Bull. Amer. Meteor. Soc*. 78:1069-79

Marshall GJ. 2003. Trends in the Southern Annular Mode from observations and reanalyses. *J. Climate*. 16:4134-43

Marshall J, Johnson H, Goodman J. 2001. A Study of the Interaction of the North Atlantic Oscillation with Ocean Circulation. *J. Climate*. 14:1399–421

Minobe S. 1997. A 50 -70 year climatic oscillation over the North Pacific and North America. *Geophys. Res. Lett.* 24:683-6

Minobe S. 1999. Resonance in Bidecadal and Pentadecadal Climate Oscillations Over the North Pacific: Role in Climatic Regime Shifts. *Geophys. Res. Lett*. 26:855-8

Moore AM, Kleeman R. 1999. Stochastic forcing of ENSO by the intraseasonal oscillation. *J. Climate*. 12:1199-220

Munnich M, Cane MA, Zebiak SE. 1991. A study of self-excited oscillations of the tropical ocean-atmosphere system. *J. Atmos. Sci.* 48:1238-48

Nakamura H, Lin HG, Yamagata T. 1997. Decadal climate variability in the North Pacific in recent decades. *Bull. Amer. Met. Soc*. 78:2215-26

Namias J, Born RM. 1974. Further studies of temporal coherence in North Pacific sea surface temperatures. *J. Geophys. Res*. 79:797-8

Newman M. 2007. Interannual to decadal predictability of tropical and North Pacific sea surface temperatures. *J. Climate*. 20:2333-56

Newman M, Compo G, Alexander MA. 2003. ENSO-forced variability of the Pacific Decadal Oscillation. *J. Climate*. 16:3853-7

Nigam S. 2003. Teleconnections. In *Encyclopedia of Atmospheric Sciences*, ed. JR Holton, JA Pyle, JA Curry, pp. 2243-69. London: Academic Press, Elsevier Science

Nobre P, Shukla J. 1996. Variations of sea surface temperature, wind stress, and rainfall over the tropical Atlantic and South America. *J. Climate*. 9:2464-79

Nonaka M, Nakamura H, Tanimoto Y, Kagimoto T, Sasaki H. 2006. Decadal variability in the Kuroshio–Oyashio Extension simulated in an eddy-resolving OGCM. *J. Climate*. 19:1970–89

North GR, Bell TL, Cahalan RF, Moeng FJ. 1982. Sampling errors in the estimation of empirical orthogonal functions. *Mon.. Wea. Rev.* 110:699-706

Palmer TN, Alessandri A, Andersen U, Cantelaube P, Davey M, et al. 2004. Development of a European multimodel ensemble system for seasonal-to-interannual prediction (DEMETER). *Bull. Amer. Meteor. Soc.* 85:853–72

Peixoto JP, Oort AH. 1992. *Physics of Climate.* American Institute of Physics, 520 pp., ISBN 0-88318-712-4

Penland C, Sardeshmukh PD. 1995. The optimal growth of tropical sea surface temperature anomalies. *J. Climate*. 8:1999-2024

Pierce DW. 2001. Distinguishing coupled ocean-atmosphere interactions from background noise in the North Pacific. *Prog. Oceanogr*. 49:331-52

Pond S, Pickard GL. 1983. *Introductory Dynamical Oceanography*. Pergamon Press. ISBN 0-75062-496-5

Power SB, Casey T, Folland C, Colman A, Mehta V. 1999. Interdecadal modulation of the impact of ENSO on Australia. *Climate Dyn.* 15:319-324

Pozo-Vázquez D, Esteban-Parra MJ, Rodrigo FS, Castro-Díez Y. 2001. The Association between ENSO and Winter Atmospheric Circulation and Temperature in the North Atlantic Region. *J. Climate*. 14:3408-20

Qiu B, Schneider N, Chen S. 2007. Coupled decadal variability in the North Pacific: An observationally-constrained idealized model. *J. Climate*. 20:3602-20

Rasmusson EM, Carpenter TH. 1982. Variations in tropical sea surface temperature and surface wind fields associated with the Southern Oscillation/El Niño. *Mon. Wea. Rev.* 110:354–84

Rayner NA, Parker DE, Horton EB, Folland CK, Alexander LV, et al. 2003. Global analyses of sea surface temperature, sea ice, and night marine air temperature since the late nineteenth century. *J. Geophys. Res.*, 108: No. D14, 4407 10.1029/2002JD002670

Saji NH, Goswami BN, Vinayachandran PN, Yamagata T. 1999. A dipole mode in the tropical Indian Ocean. *Nature*. 401:360–3

Schlesinger ME, Ramankutty N. 1994. An oscillation in the global climate system of period 65-70 years. *Nature*. 367:723-6

Schneider N, Cornuelle BD. 2005. The forcing of the Pacific Decadal Oscillation. *J. Climate*. 18:4355-73

Schopf PS, Suarez MJ. 1988. Vacillations in a coupled ocean-atmosphere model. *J. Atmos. Sci.* 45:549-66

Schott FA, Xie S-P, McCreary JP. 2009. Indian Ocean circulation and climate variability. *Rev. Geophys*. 47, RG1002, doi:10.1029/2007RG000245

Sen Gupta A, England MH. 2007. Coupled ocean-atmosphere feedback in the Southern Annular Mode. *J. Climate*. 20:3677-92

Shinoda T, Hendon HH, Alexander MA. 2004. Surface and subsurface dipole variability in the Indian Ocean and its relation with ENSO. *Deep-Sea Res*. 51:619–35

Stewart RH. 2005. Introduction to Physical Oceanography. Open Source Textbook. http://oceanworld.tamu.edu/resources/ocng_textbook/contents.html

Taguchi B, Xie S-P, Schneider N, Nonaka M, Sasaki H, Sasai Y. 2007. Decadal variability of the Kuroshio Extension: Observations and an eddy-resolving model hindcast. *J. Climate*. 20:2357–77

Thompson CJ, Battisti DS. 2001. A Linear Stochastic Dynamical Model of ENSO. Part II: Analysis. *J. Climate*. 14:445-66.

Thompson DWJ, Wallace JM. 2000. Annular modes in the extratropical circulation. Part I: Month-to-month variability. *J. Climate*, 13:1000-16

North GR, Bell TL, Cahalan RF, Moeng FJ. 1982. Sampling errors in the estimation of empirical orthogonal functions. *Mon. Wea. Rev.* 110:699 -706

Thompson DWJ, Kennedy JJ, Wallace JM, Jones PD. 2008. A large discontinuity in the mid-twentieth century in observed global-mean surface temperature. *Nature*. 453(29), doi:10.1038/nature06982

Ting M, Kushnir Y, Seager R, Li C. 2009. Forced and Internal Twentieth-Century SST Trends in the North Atlantic. *J. Climate*. 22:1469–81

Trenberth KE, Branstator GW, Karoly D, Kumar A, Lau N-C, Ropelewski C. 1998. Progress during TOGA in understanding and modeling global teleconnections associated with tropical sea surface temperatures. *J. Geophys. Res*. 103:14291-324

Vallis GK. 2006. *Atmospheric and Oceanic Fluid Dynamics*. Cambridge University Press, 745 pp.

Venegas SA, Mysak LA, Straub DN. 1997. Atmosphere-ocean coupled variability in the South Atlantic. *J. Climate*. 10:2904-20

Vimont DJ. 2005. The contribution of the interannual ENSO cycle to the spatial pattern of ENSO-like decadal variability. *J. Climate*. 18:2080-92

Vimont DJ, Kossin JP. 2007. The Atlantic Meridional Mode and hurricane activity. *Geophys. Res. Lett.* 34, L07709, doi:10.1029/2007GL029683

Visbeck M, Chassignet EP, Curry RG, Delworth TL, Dickson RR, Krahmann K. 2003. The ocean's response to North Atlantic Oscillation variability. In *The North Atlantic Oscillation: Climatic Significance and Environmental Impact*, pp. 113-146. Geophys. Monogr., Vol. 134, Amer. Geophys. Union

von Storch H, Zwiers FW. 1999. *Statistical Analysis in Climate Research,* Cambridge University Press

Walker GT, Bliss EW. 1932: World Weather V. *Mem. Roy. Met. Soc*. 4:53-84

Wallace JM, Gutzler DS. 1981. Teleconnections in the geopotential height field during the Northern Hemisphere winter. *Mon. Wea. Rev*. 109:784-812

Wang C, Enfield DB, Lee S-K, Landsea CW. 2006. Influences of the Atlantic warm pool on Western Hemisphere summer rainfall and Atlantic hurricanes. *J. Climate*. 19: 3011-28

Watanabe M, Kimoto M. 2000. Atmosphere-ocean thermal coupling in the North Atlantic: A positive feedback. *Q. J. R. Meteorol. Soc.* 126:3343-69

Wood RA, Keen AB, Mitchell JFB, Gregory JM. 1999. Changing spatial structure of the thermohaline circulation in response to atmospheric CO2 forcing in a climate model. *Nature*. 399:572-5

Xie S-P, Annamalai H, Schott FA, McCreary JP. 2002. Structure and mechanisms of South Indian Ocean climate variability. *J. Climate*. 15:864-78

Xie S-P, Carton JA. 2004. Tropical Atlantic variability: Patterns, mechanisms, and impacts. In *Earth Climate: The Ocean-Atmosphere Interaction*, ed. C Wang, S-P Xie, JA Carton, 121-142. Washington D.C.: Geophys. Monograph, 147, AGU

Xie S-P, Hu K, Hafner J, Tokinaga H, Du Y, Huang G, Sampe T. 2009. Indian Ocean capacitor effect on Indo-western Pacific climate during the summer following El Nino. *J. Climate*. 22:730–47

Xie S-P, Tanimoto Y. 1998. A pan-Atlantic decadal climate oscillation. *Geophys. Res. Lett*. 25:2185-8

Zebiak SE. 1993. Air-sea interaction in the equatorial Atlantic region. *J. Climate*. 6:1567-86.

Zebiak SE, Cane MA. 1987. A model El Nino-Southern Oscillation. *Mon. Wea. Rev.* 115:2262-78

Zhang Y, Wallace JM, Battisti DS. 1997. ENSO-like interdecadal variability. *J. Climate*. 10:1004-20

Key Terms

1. Upper ocean mixed layer (section 2a)

2. Ekman pumping (section 2a)

3. Ekman current (section 2a)

4. White noise (section 2b)

5. Potential predictability (section 2b)

6. Re-emergence mechanism (section 2b)

7. Ships-of-opportunity (section 3)

8. Madden-Julian oscillation (section 5ai)

Figure Captions

Figure 1. Anomaly patterns associated with a +1 standard deviation departure of the North Atlantic Oscillation (NAO) Index during winter (December-March). (*a*) SST (shading), SLP (contours) and surface wind (vectors). (*b*) Sensible plus latent energy flux (shading), SLP (contours) and surface wind (vectors). (*c*) Ekman heat transport expressed as an equivalent surface energy flux (shading), long-term mean SST (contours) and Ekman currents (vectors). (*d*) Sum of the sensible, latent and Ekman energy fluxes (shading), SLP (contours) and surface wind (vectors). The SLP contour interval is 1 hPa, with negative values dashed.

Figure 2. Illustration of the stochastic climate model paradigm. The top curve shows a random (e.g., "white noise") atmospheric heat flux forcing time series. The middle and bottom curves show the upper ocean mixed layer temperature response for a mixed layer depth of 75m (middle) and 500m (bottom). Note the slow fluctuations in the ocean mixed layer temperature response.

Figure 3. Distribution of SST observations from the International Comprehensive Ocean Atmosphere Data Set for each 20 year period since 1860. Color shading indicates the percentage of months with at least 1 measurement in a 2 º latitude by 2 º longitude grid box.

Figure 4. (Top) Long-term mean SST distribution from satellite passive microwave measurements during 1982-2008. (Bottom) The standard deviation of monthly SST anomalies (deviations from the long term monthly means) based on the same data set.

Figure 5. (Top) Leading Empirical Orthogonal Function (EOF) of detrended monthly SST anomalies over the global oceans based on the HadISST data set during 1900-2008. This mode, which accounts for 19% of the variance, depicts the El Niño/Southern Oscillation phenomenon. (Middle) Monthly SST anomaly time series in the Niño3.4 region (5°N–5°S, 170°–120°W: outlined by the rectangle on the EOF pattern). (Bottom) left: Power spectrum of the Niño3.4 SST anomaly time series based on 1950-2008 (solid curve) and 1900-2008 (dashed curve); right: monthly standard deviation of the Niño3.4 SST anomaly time series.

Figure 6. Composite ENSO evolution of seasonal SST (shading) and SLP (contours) anomalies starting in March-May of year 0 (MAM0) and ending with June-August of the following year (JJA1). The SLP contour interval is 1 hPa, with negative values dashed. See text for details.

Figure 7. (Top) First and second EOFs of detrended monthly SST anomalies in the Tropical Indian Ocean based on the HadISST data set during 1900-2008. These modes account for 39% and 12% of the variance, respectively. EOF1 depicts the basin-wide mode and EOF2 depicts the dipole mode. (Bottom) Monthly standard deviations of the PC time series associated with EOF1 (green) and EOF2 (blue).

Figure 8. (Top) First and second EOFs of detrended monthly SST anomalies in the Tropical Atlantic Ocean based on the HadISST data set during 1900-2008. These modes account for 38% and 25% of the variance, respectively. EOF1 depicts the Atlantic Niño mode and EOF2 depicts the meridional mode. (Bottom) Monthly standard deviations of the PC time series associated with EOF1 (green) and EOF2 (blue).

Figure 9. SST (shading) and 500 hPa geopotential height (contours) anomaly patterns associated with the leading PC time series of monthly SST anomalies in the Southern Hemisphere (south of 20°S) during November-March (left) and May-October (right). The contours are drawn at +/- 35m, 25m, 15m, and 5m, with negative values dashed. Reprinted with permission from Ciasto and Thompson (2008).

Figure 10. Pacific Decadal Oscillation. (Top) The leading EOF of monthly SST anomalies over the North Pacific (after removing the global mean SST anomaly) based on the HadISST data set during 1900-2008. Although the EOF calculation was restricted to the North Pacific (region outlined by the black rectangle), the pattern is displayed globally by regressing the monthly SST anomalies at each location upon the PC time series. (Bottom) Associated PC time series (the unsmoothed record is shown by the red and blue bars, and the 5 year running mean record is shown by the black curve).

Figure 11. Atlantic Multidecadal Oscillation. (Top) Regression pattern of monthly SST anomalies (after removing the global mean SST anomaly) upon the North Atlantic SST

Index, based on the HadISST data set during 1870-2008. (Bottom) The North Atlantic SST Index, defined as the average monthly SST anomaly over the North Atlantic (0°-70°N) minus the global mean monthly SST anomaly (red and blue bars). The green curve depicts an estimate of the natural component of the 10 year low-pass filtered North Atlantic SST Index from Ting et al. (2009).

Figures

Table 1. Commonly used SST data sets for climate studies.

Name and Web Address	Period of Record	Coverage	Comments
ICOADS ***http://icoads.noaa.gov/***	1800-present	Monthly 2°x2° since 1800 1°x1° since 1960	In situ data. No processing beyond quality control.
HadISST ***http://badc.nerc.ac.uk/data/hadisst/***	1870-present	Monthly 1°x1°	In situ/satellite data. Missing values filled.
NCDC ***http://www.ncdc.noaa.gov/oa/climate/ research/sst/ersstv3.php***	1854-present	Monthly 2°x2°	In situ/satellite data. Missing values filled.
NOAA Optimum Interpolation ***http://www.emc.ncep.noaa.gov/research/ cmb/sst_analysis/***	Nov. 1981-present	Weekly / Monthly 1°x1°	Satellite estimates.
NOAA Optimum Interpolation ¼ Degree Daily SST Analysis ***http://www.ncdc.noaa.gov/oa/climate/ research/sst/oi-daily.php***	Sep. 1981-present	Daily .25°x.25°	Satellite estimates.
Kaplan Extended v2 SST Anomaly Data ***http://ingrid.ldeo.columbia.edu/SOURCES /.KAPLAN/.EXTENDED/.v2/.ssta/***	1856-present	Monthly 5°x5°	In situ/satellite data. Missing values filled.

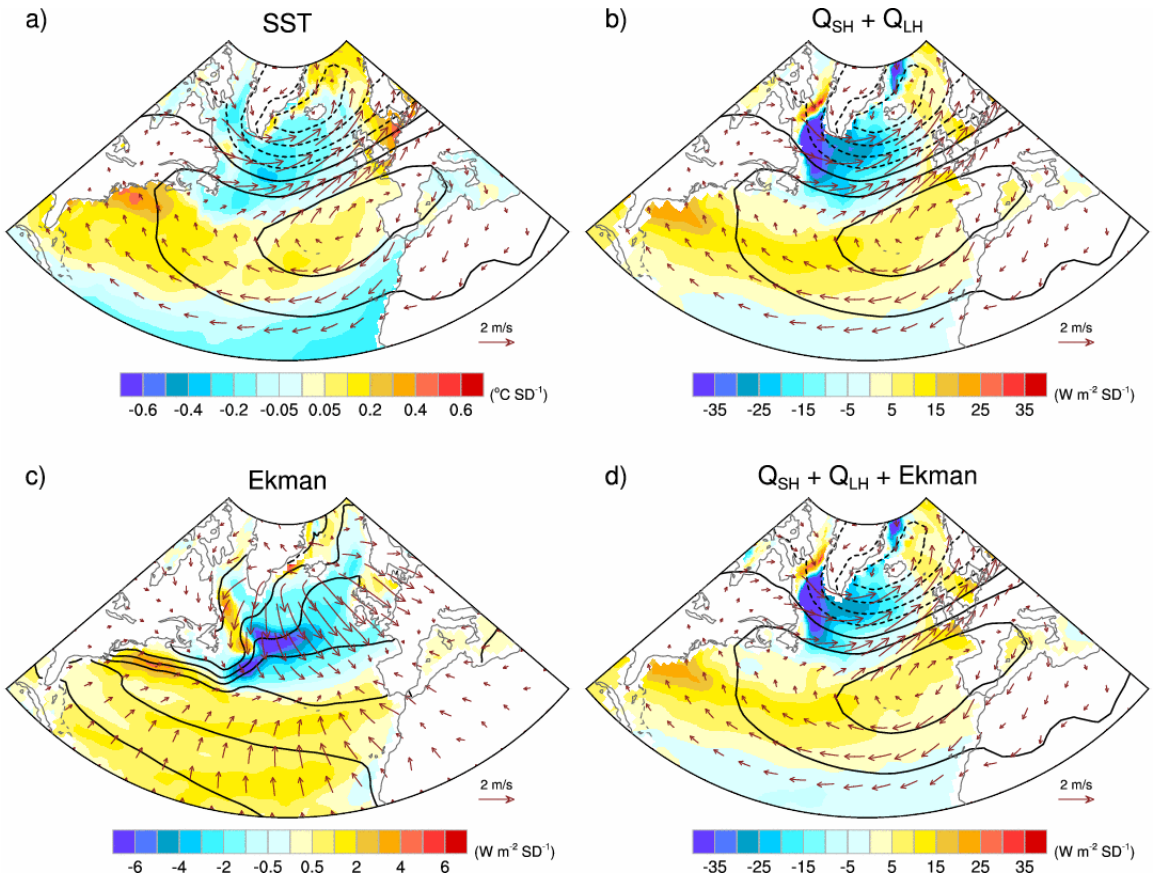

Figure 1. Anomaly patterns associated with a +1 standard deviation departure of the North Atlantic Oscillation (NAO) Index during winter (December-March). (*a*) SST (shading), SLP (contours) and surface wind (vectors). (*b*) Sensible plus latent energy flux (shading), SLP (contours) and surface wind (vectors). (*c*) Ekman heat transport expressed as an equivalent surface energy flux (shading), long-term mean SST (contours) and Ekman currents (vectors). (*d*) Sum of the sensible, latent and Ekman energy fluxes (shading), SLP (contours) and surface wind (vectors). The SLP contour interval is 1 hPa, with negative values dashed.

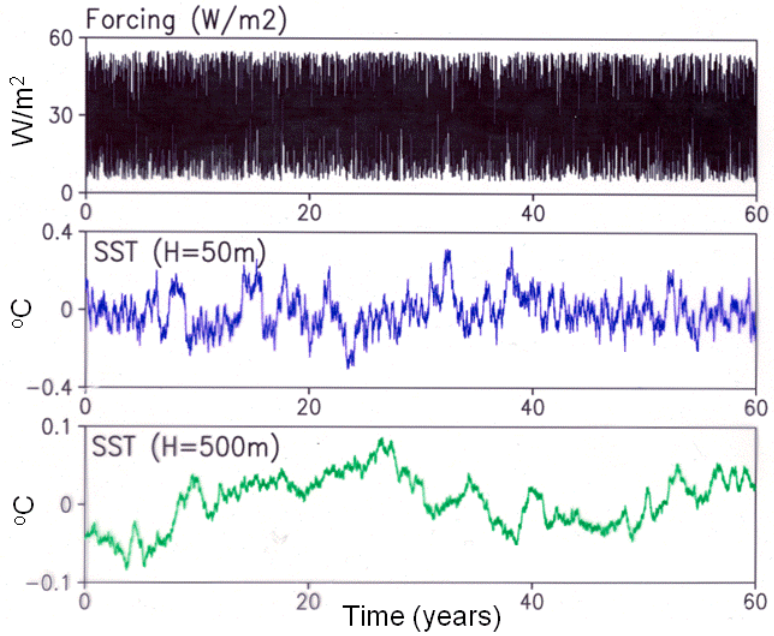

Figure 2. Illustration of the stochastic climate model paradigm. The top curve shows a random (e.g., "white noise") atmospheric heat flux forcing time series. The middle and bottom curves show the upper ocean mixed layer temperature response for a mixed layer depth of 75m (middle) and 500m (bottom). Note the slow fluctuations in the ocean mixed layer temperature response.

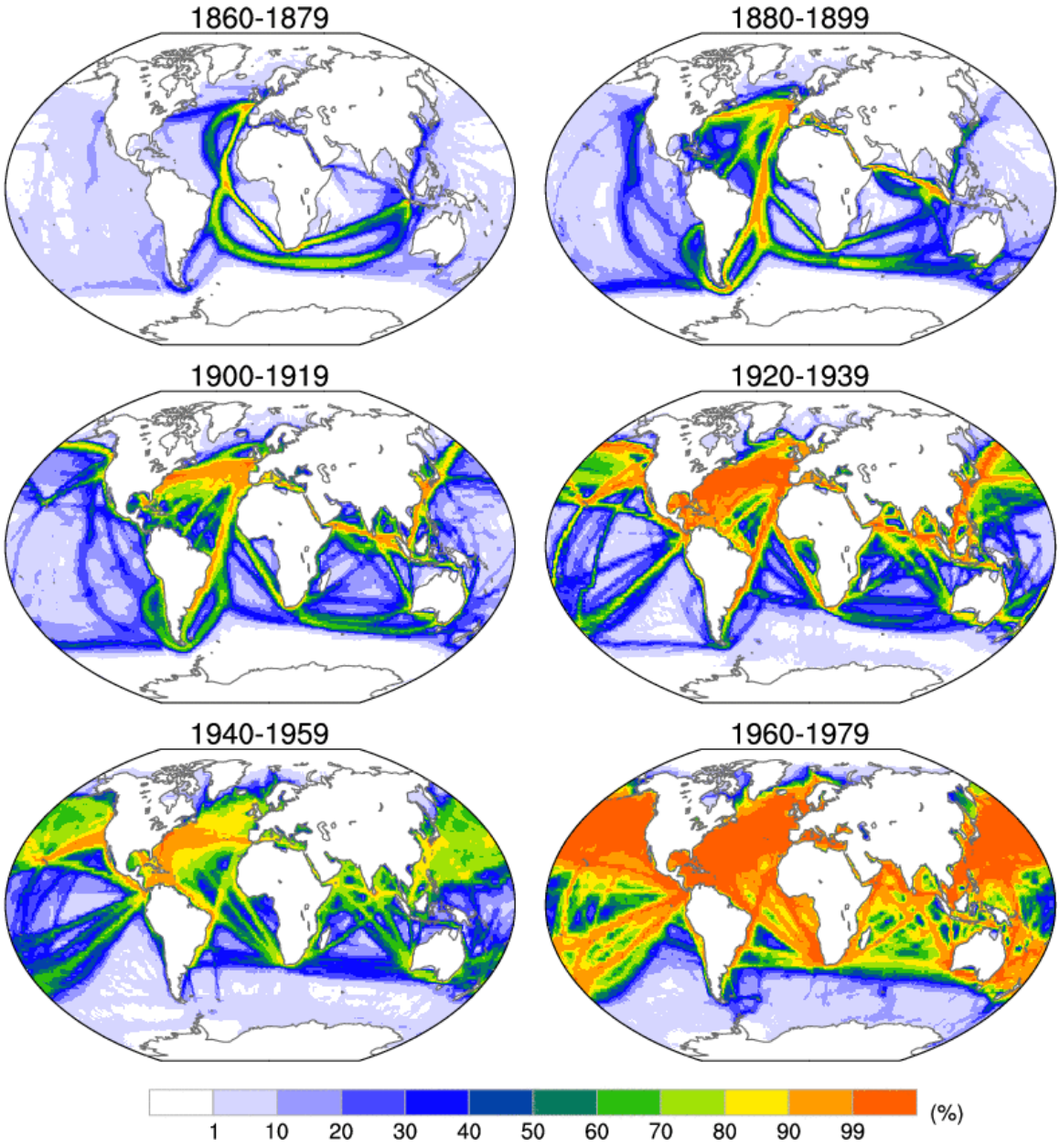

Figure 3. Distribution of SST observations from the International Comprehensive Ocean Atmosphere Data Set for each 20 year period since 1860. Color shading indicates the percentage of months with at least 1 measurement in a 2 º latitude by 2 º longitude grid box.

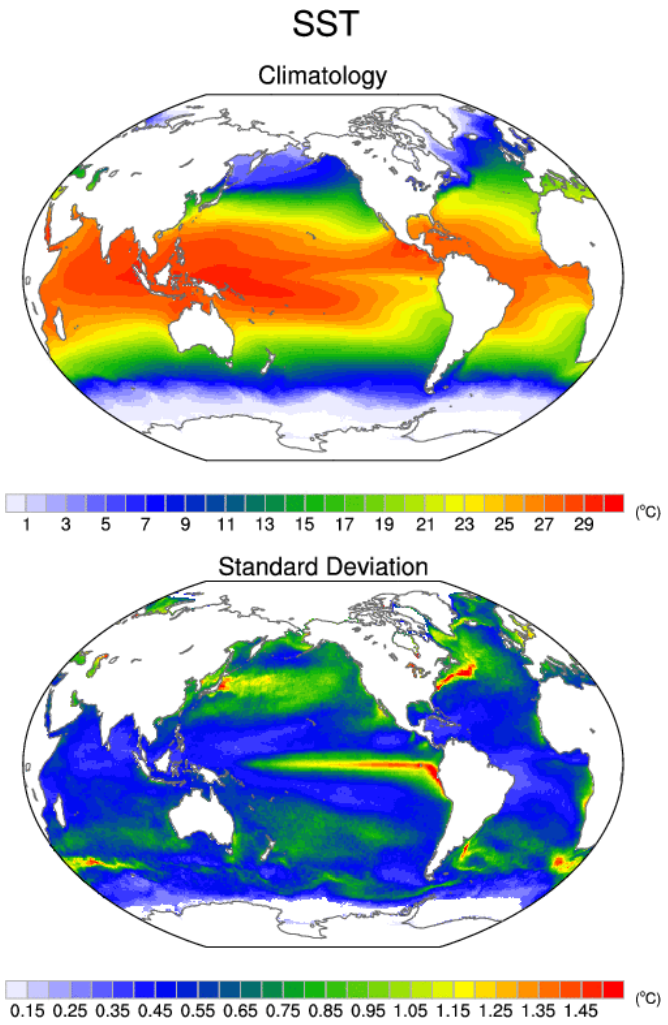

Figure 4. (Top) Long-term mean SST distribution from satellite passive microwave measurements during 1982-2008. (Bottom) The standard deviation of monthly SST anomalies (deviations from the long term monthly means) based on the same data set.

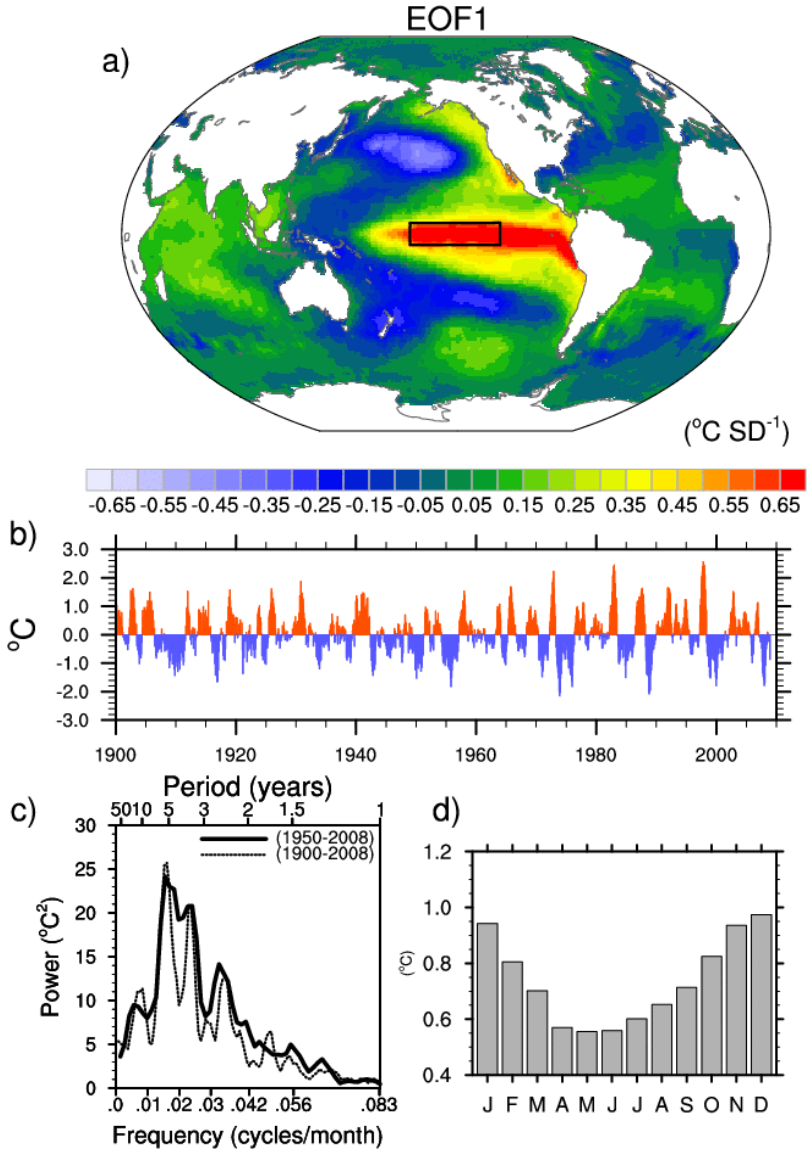

Figure 5. (Top) Leading Empirical Orthogonal Function (EOF) of detrended monthly SST anomalies over the global oceans based on the HadISST data set during 1900-2008. This mode, which accounts for 19% of the variance, depicts the El Nino/Southern Oscillation phenomenon. (Middle) Monthly SST anomaly time series in the Nino3.4 region (5°N–5°S, 170°–120°W: outlined by the rectangle on the EOF pattern). (Bottom) left: Power spectrum of the Nino3.4 SST anomaly time series based on 1950-2008 (solid curve) and 1900-2008 (dashed curve); right: monthly standard deviation of the Nino3.4 SST anomaly time series.

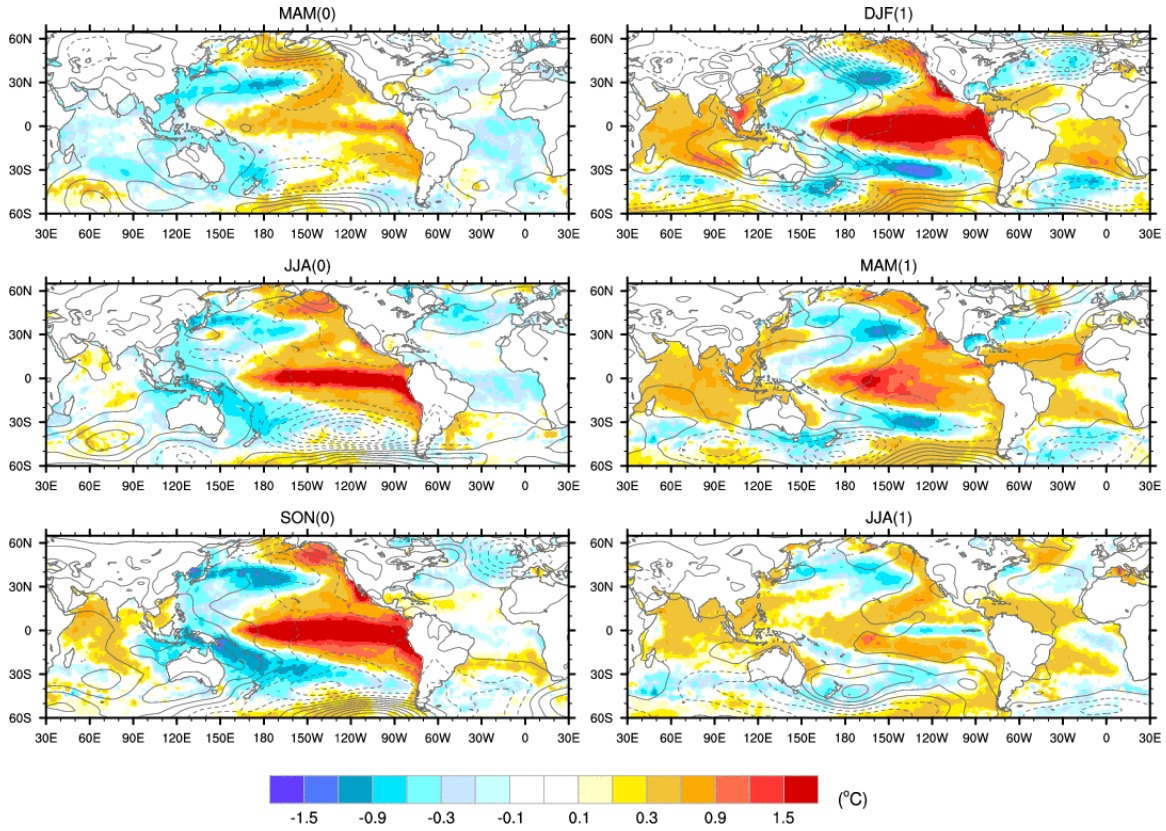

Figure 6. Composite ENSO evolution of seasonal SST (shading) and SLP (contours) anomalies starting in March-May of year 0 (MAM0) and ending with June-August of the following year (JJA1). The SLP contour interval is 1 hPa, with negative values dashed. See text for details.

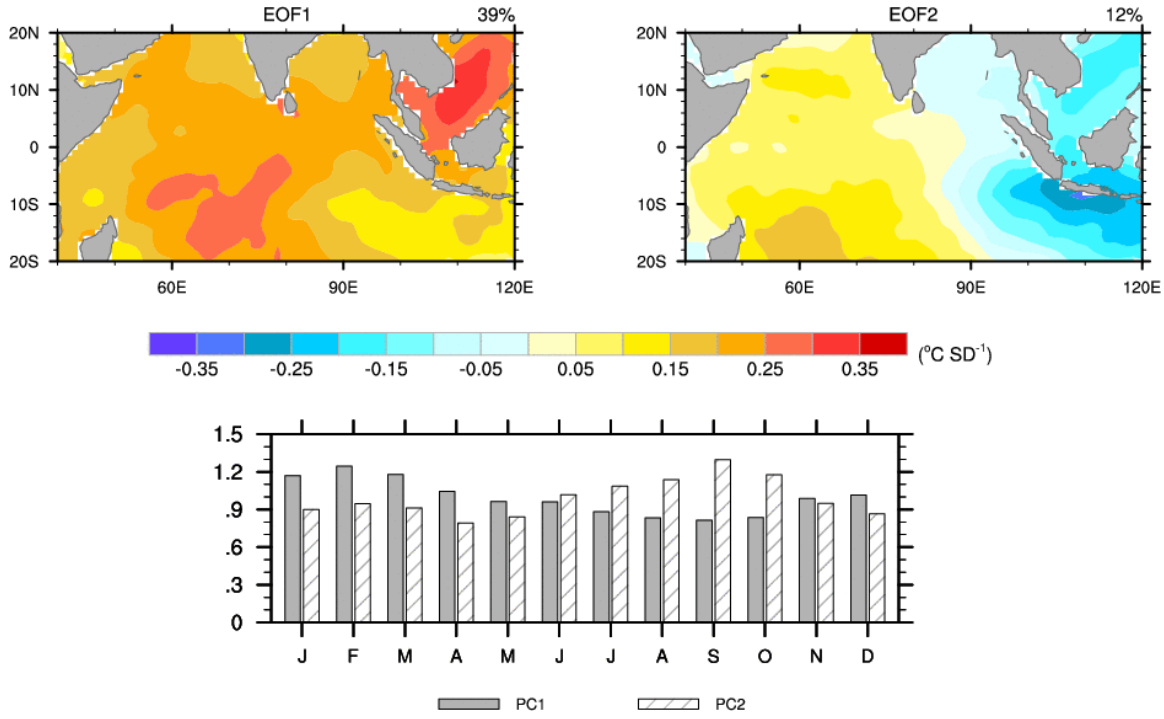

Figure 7. (Top) First and second EOFs of detrended monthly SST anomalies in the Tropical Indian Ocean based on the HadISST data set during 1900-2008. These modes account for 39% and 12% of the variance, respectively. EOF1 depicts the basin-wide mode and EOF2 depicts the dipole mode. (Bottom) Monthly standard deviations of the PC time series associated with EOF1 (green) and EOF2 (blue).

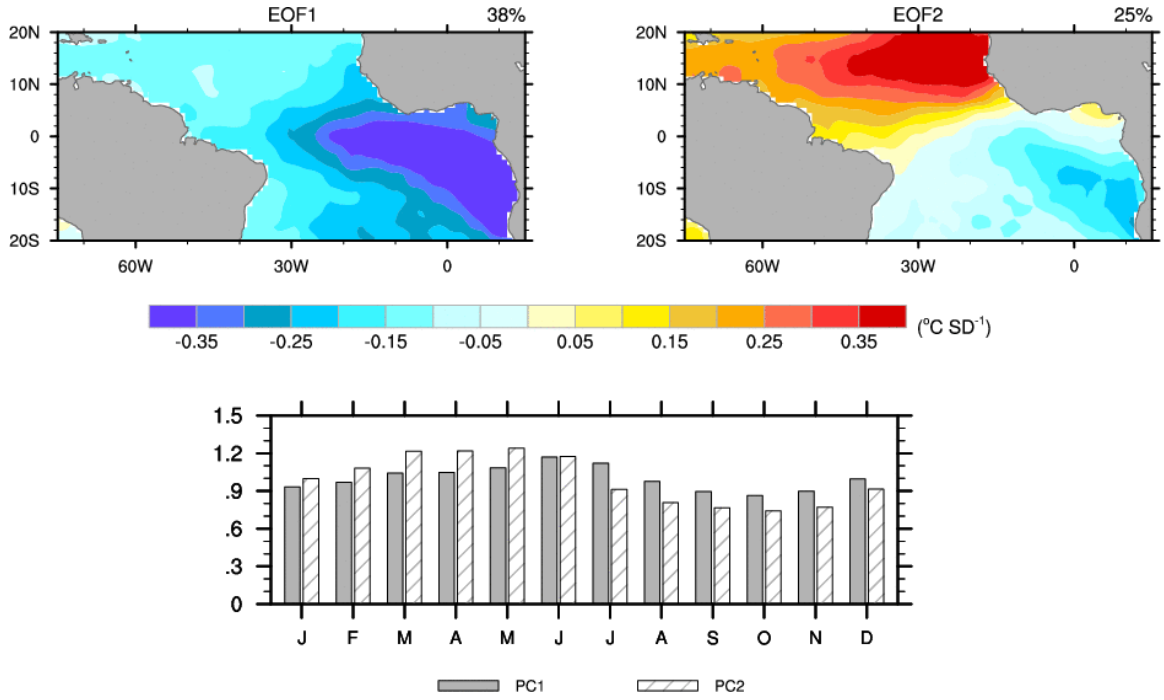

Figure 8. (Top) First and second EOFs of detrended monthly SST anomalies in the Tropical Atlantic Ocean based on the HadISST data set during 1900-2008. These modes account for 38% and 25% of the variance, respectively. EOF1 depicts the Atlantic Nino mode and EOF2 depicts the meridional mode. (Bottom) Monthly standard deviations of the PC time series associated with EOF1 (green) and EOF2 (blue).

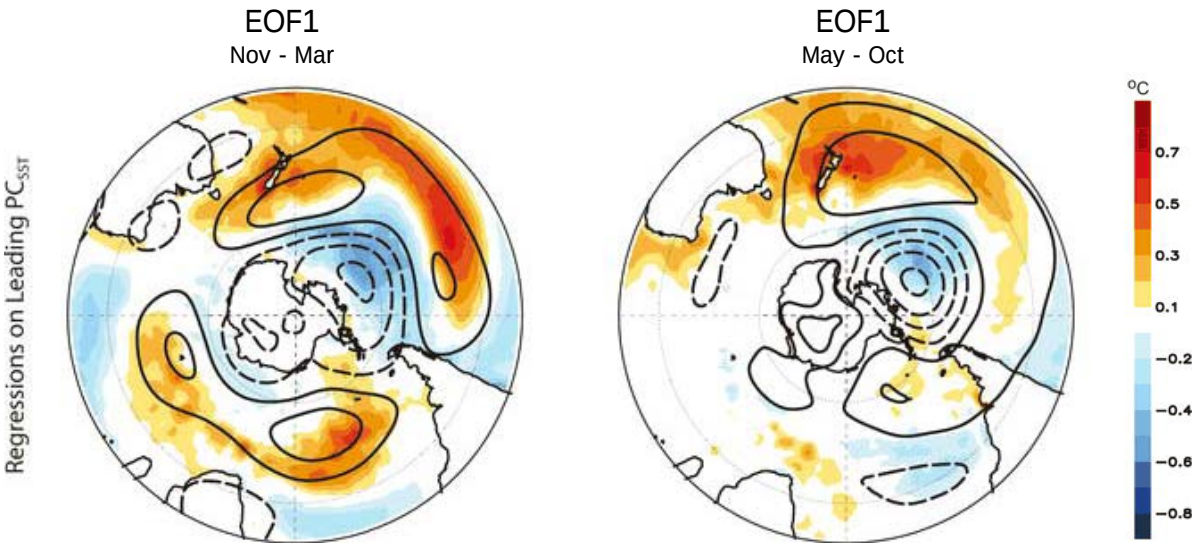

Figure 9. SST (shading) and 500 hPa geopotential height (contours) anomaly patterns associated with the leading PC time series of monthly SST anomalies in the Southern Hemisphere (south of 20°S) during November-March (left) and May-October (right). The contours are drawn at +/- 35m, 25m, 15m, and 5m, with negative values dashed. Reprinted with permission from Ciasto and Thompson (2008).

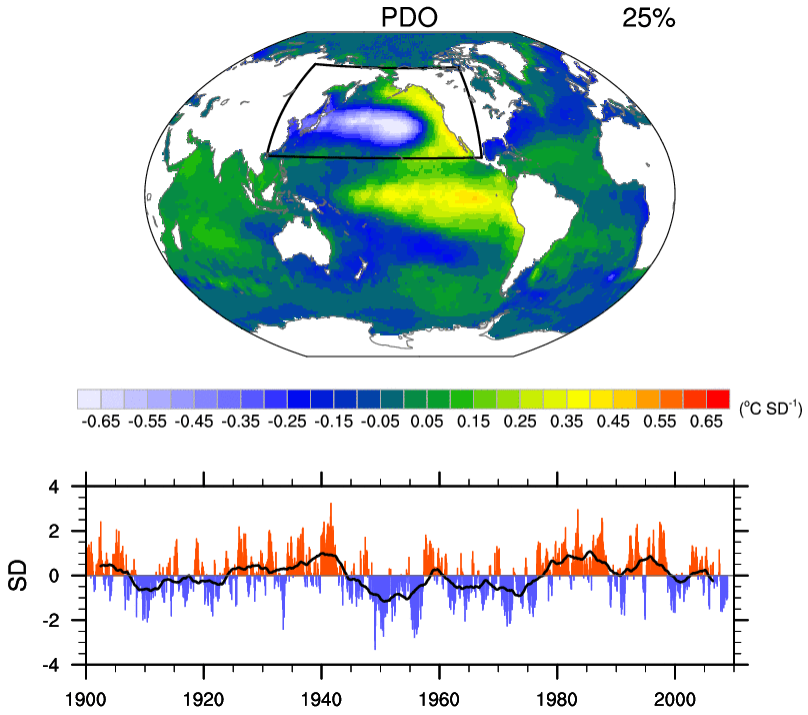

Figure 10. Pacific Decadal Oscillation. (Top) The leading EOF of monthly SST anomalies over the North Pacific (after removing the global mean SST anomaly) based on the HadISST data set during 1900-2008. Although the EOF calculation was restricted to the North Pacific (region outlined by the black rectangle), the pattern is displayed globally by regressing the monthly SST anomalies at each location upon the PC time series. (Bottom) Associated PC time series (the unsmoothed record is shown by the red and blue bars, and the 5 year running mean record is shown by the black curve).

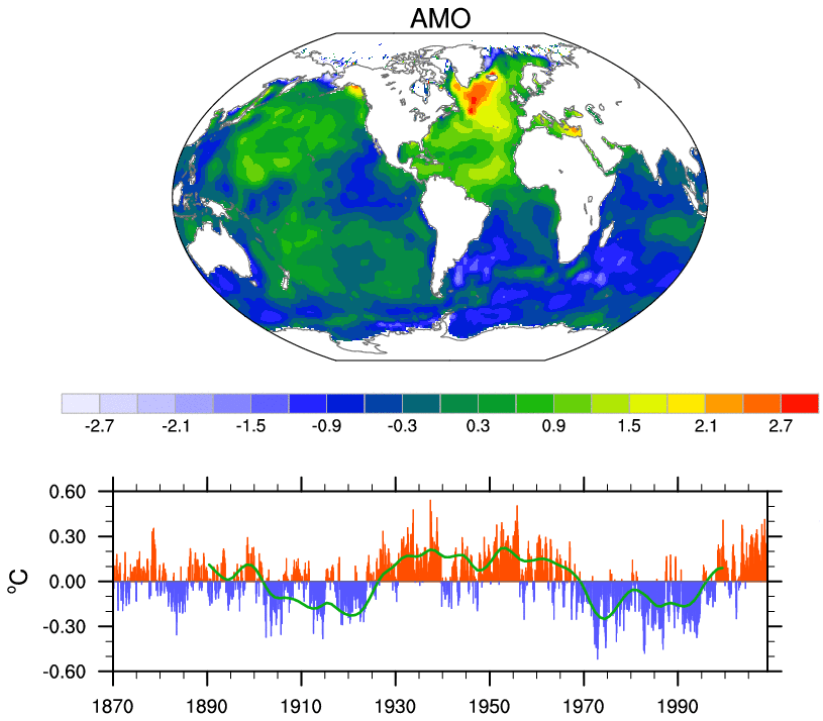

Figure 11. Atlantic Multidecadal Oscillation. (Top) Regression pattern of monthly SST anomalies (after removing the global mean SST anomaly) upon the North Atlantic SST Index, based on the HadISST data set during 1870-2008. (Bottom) The North Atlantic SST Index, defined as the average monthly SST anomaly over the North Atlantic (0°-70°N) minus the global mean monthly SST anomaly (red and blue bars). The green curve depicts an estimate of the natural component of the 10 year low-pass filtered North Atlantic SST Index from Ting et al. (2009).